CR-137793

FUNDAMENTAL STUDIES ON THE NATURE AND PROPERTIES OF CERAMIC FIBER INSULATION

BY

J. I. Mueller, O. J. Whittemore, Jr., W. D. Scott,
A. D. Miller, L. W. Smiser and D. B. Leiser

Prepared under Contract No. NAS 2-6541
UNIVERSITY OF WASHINGTON
Seattle, Washington 98195

for

NATIONAL AERONAUTICS AND SPACE ADMINISTRATION
AMES RESEARCH CENTER

CONTENTS

LIST OF TABLES

LIST OF FIGURES

SYMBOLS

D	diameter
D_o	initial diameter
$\overline{D}_p$	mean pore diameter
E	activation energy for viscous flow
L	unsupported length of fiber
M	modulus of rupture
nm	not measured
P	load at failure
R	ideal gas constant
S_L	linear shrinkage
t	time
T	temperature
V_{fc}	volume fraction cristobalite
V_p	pore volume
$x - y$	measured in horizontal plane
z	measured in vertical plane
γ	surface tension
η	viscosity
θ	wetting angle
ρ_b	bulk density
ρ_t	true density
σ	tensile strength
σ_{max}	maximum stress in tension
%	weight percent

Subscripts:

b	bulk
fc	fraction cristobalite
L	linear
max	maximum
o	initial
p	pore
t	true

FUNDAMENTAL STUDIES ON THE NATURE AND PROPERTIES OF CERAMIC FIBER INSULATION

J. I. Mueller, O. J. Whittemore, Jr., W. D. Scott,
A. D. Miller, L. W. Smiser,* and D. B. Leiser†

University of Washington

SUMMARY

Silica and mullite fibers used to fabricate reusable surface insulation (RSI) for the space shuttle orbiter may devitrify/recrystallize within the temperature range anticipated upon re-entry. Studies of silica fibers show this to be dependent upon impurity level, temperature, and time at temperature. It was determined that the effects of the material improvement and optimization program were positive. The degree of crystallinity is shown to have a predominant effect upon the strength of fabricated RSI tile, and limits are determined. Models are developed to predict tensile strengths and shrinkage rates of silica tile based upon readily measurable parameters. Thermal cycling which simulates re-entry results in an increase in the crystallinity and in the porosity of tile coatings.

---

*Materials and Process Engineer, Rockwell International, Downey, California.

†Research Associate, Stanford University, Palo Alto, California.

INTRODUCTION

The consideration in 1970 that a rigidized ceramic external insulation might be employed as a reusable thermal protection system for the shuttle vehicles resulted in the use of private and public funds to further develop such a material and to initiate appropriate tests for determining its feasibility. Considerable progress had been made in the development of materials for this purpose, but fundamental investigations regarding the nature of the beginning materials and the final product had not been studied in depth. Materials improvement and optimization were dependent upon an understanding of such basic knowledge as the effect of temperature upon the chemical and structural stability of the material to be used, the effect of cyclic temperature changes upon phase transformations, and their effects, in turn, upon mechanical integrity.

As part of the shuttle thermal protection system, this material is required to withstand 100 cycles of oxidizing temperatures of up to 1640 K (2300°F) on exterior surfaces and to have the insulation characteristics needed to limit the back-face temperature to less than 570 K (350°F). The effects of devitrification/crystallization can be quite profound within this range, especially in silica, because the devitrification product may be either α-quartz, α-cristobalite, or a combination of both. Each of these crystalline phases has an $\alpha - \beta$ inversion at low temperatures, and with each is associated a significant volume expansion/contraction, depending upon the direction of the inversion. The quartz transformation occurs at 846 K (1063°F), while the cristobalite transformation occurs at approximately 470 K (390°F). If no devitrification takes place, low-thermal-

expansion silica glass is present. If devitrification does take place, cristobalite is less desirable because its inversion temperature is totally within the temperature range of the entire thickness of the insulation layer. The presence of either cristobalite or quartz, however, might affect the mechanical properties of the insulation after several re-entry cycles, and some knowledge of the devitrificaion reaction and reaction products was obviously needed.

The Ceramic Materials Research Program at the University of Washington, supported principally by NASA Grant NGL 48-002-004, had initiated a small program in 1970 to obtain preliminary information on the nature of silica and mullite fibers. In April 1971, the Ames Research Center awarded Contract NAS 2-6541 to the University in order to expand the earlier program. Its purpose was to obtain such fundamental information as would be helpful in improvement and optimization. This effort gained greater significance in late 1971 when the decision was made to baseline this material -- to be known as reusable surface insulation (RSI) -- as the thermal protection system (TPS) for the space shuttle vehicle. The research program was divided into five tasks, as follows:

1. "Study of Thermal Environment on 'As-Received' Fibers." The objectives were to determine the effects of composition, temperature, and time upon the devitrification/crystallization of the fibers upon their morphology.

2. "Study of 'As-Received' Uncoated Tile." The primary purpose of this task was to ascertain the effects of processing upon the crystallinity of the tile.

3. "Study of Thermal Environment on Uncoated Tile." This task was to determine the effects of isothermal and simulated re-entry heating upon the crystalline and mechanical properties of the tile.

4. "Study of the Coating-Tile Reaction." This was a study initiated to determine the presence or absence of any interfacial reaction zone and of possible reaction products. It was also hoped that this study would determine the nature of the bonding behavior of the tile and the coating.

5. "Study of Thermal Environment on Coated Tiles." This task was similar to number three in that it would lead to information regarding the effect of isothermal and cyclic heating upon the coating and coating/tile interaction.

Although the research was performed as separate tasks, this report does not focus on the individual tasks themselves. Rather, it is organized to present information concerning the specific nature and properties of RSI.

Further, it should be noted that, in the beginning, the research was concerned with both silica and mullite fibers and the tiles produced using them. However, after a NASA decision in early 1973 to confine development to silica fiber products, efforts were limited to these materials.

While the research was in progress, extensive data were generated and made available in quarterly reports from the contractor. This report will deal primarily with the information considered to be most significant to the present and future development of RSI.

DESCRIPTION OF MATERIALS

A description of the materials which were under study must be limited to the information which was available to the investigators, for much of the data on composition and processing were proprietary.

REUSABLE SURFACE INSULATION

Both aerospace and industrial requirements in the late 1960's and early 1970's resulted in the development of light-weight, rigidized refractory insulation materials manufactured from ceramic fibers of various compositions. These were self-supporting and, depending upon their composition, had the capability of withstanding oxidation and deformation at sustained temperatures ranging from 1530 K (2700°F) to 2970 K (4900°F). The thermal protection system required by the space shuttle led to the consideration that this type of material might be a suitable candidate. In order to meet design specifications, however, it was necessary to develop an appropriate water repellent coating for the tile; moreover, both coating and tile had to be capable of withstanding the re-entry conditions for 100 missions. These re-entry conditions included exposure to severe thermal stress convective heating for which conventional materials were not necessarily appropriate.

RSI tiles are fabricated from ceramic fibers whose diameters are in the 0.5 to 8 μm range. Initially these were both off-the-shelf and developmental materials. Figures 1 and 2 are scanning electron photomicrographs of typical "as-received" fibers. Although each contractor

had his own particular method of processing, in general the fibers were chopped, dispersed in a water slurry, and dewatered by vacuum filtration or centrifugal casting to the desired size and shape, after which they were dried at a moderate temperature. The binder was added to the slurry or, in some cases, was added by "wicking" through the dried tile, which was then re-dried. The tile was fired to develop the rigidized structure. Early densities of RSI tiles ranged from 220 to 290 kg/m^3 (14 to 18 pounds per cubic foot). Subsequently, RSI with a density of 140 kg/m^3 (9 pounds per cubic foot) was baselined, but no samples of this type were studied in the research being reported here. Coatings were then applied by spraying, and the tile was refired. The composition of the coatings was developed to produce a water-resistant material with a suitable emissivity and a coating whose thermal expansion would match as closely as possible that of the tile. Figure 3 shows RSI tile in each of the principal steps of processing.

FIBERS

Although several types of ceramic fiber materials were investigated, this report will deal only with the two principal materials, silica and mullite. Furthermore, because there was one primary source for each material, only the fibers from these two sources will be described.

Silica

The silica fiber studied was a high purity (99+%), vitreous material manufactured by Johns-Manville Corporation under the registered trade name

Microquartz. Although the processing details are proprietary, it is known that all the fibers investigated in this study were made from a common glass batch. The batch was melted, then formed into marbles. A given lot of fiber was produced by melting a number of these marbles and drawing the fibers, which were then acid leached to reduce the impurities of the original glass. In the discussions which follow references are made to various lot numbers. Some experiments were undertaken by the manufacturer to improve the fiber from the marble remelt process forward. Each of these was given a specific lot number. This is the reason that early fiber lots (pre-1971) had higher impurity levels than subsequent lots. The majority of the fiber diameters were in the range from 0.5 to 1.3 μm, with the mean at about 1.1 μm.

All silica fibers were furnished by the NASA centers or their contractors. No fiber was received directly from Johns-Manville. Attempts were made to obtain fiber samples from the same lots from which tile was produced, but these, unfortunately, were unobtainable. The "as-received" fiber was loosely packed in a random manner. Qualitative x-ray diffraction examination indicated that all except some early samples were completely vitreous. A few of the early samples showed α-quartz to be present in trace amounts.

Mullite

The mullite fibers used were produced by the Babcock-Wilcox Company. The fibers were formed from a gel, the final composition of which was close to that of the mineral mullite -- $3Al_2O_3 \cdot 2SiO_2$. Chemical analyses of some

of the original fibers indicated a composition slightly on the alumina side of stoichiometric mullite. The extruded material was probably fired to a moderate temperature in order to produce a fiber of sufficient strength for handling and working and to eliminate certain volatile components.

The "as-received" fibers ranged in diameter from 1 to 17 μm, with an average size of about 7.5 μm. X-ray diffraction analysis indicated that the material was principally non-crystalline, although some mullite and a γ-Al_2O_3-type material were observed.

PROCESSED TILE

The term "processed tile" refers to a rigid shape, formed from micron-sized ceramic fibers with or without a binder and/or other additives, and fired to a temperature which develops an appropriate bond between the fibers. For the purposes of this report, it will be assumed that tiles are uncoated, for they and their coatings will be discussed separately.

All tile samples were received from NASA centers or directly from their contractors on order of a NASA center. Although the tiles studied in the latter part of the program were readily identifiable as to date of manufacture and fiber lot designation, not all tiles obtained in the early period of the work were identified in this manner. The description which follows is by manufacturer and fiber type. Parenthetical references are made to appropriate pages in NASA TM X-2719 which describe certain of the processing details.

One of the early difficulties in this and other efforts attempting to evaluate progress and improvements due to rapidly moving developments in

the RSI program was the lack of a baseline material. In September 1972, each contractor was requested by NASA to designate a baseline material, and these materials will be noted in this report.

Silica

Ames Research Center (AIM)

The Ames samples were fabricated by the Thermal Protection Branch, NASA-Ames Research Center, Moffett Field, California, using Microquartz fibers with a mixture of Cab-o-Sil, starch, and ammonia as a binder [TM X-2719, p. 1170].

General Electric Company (REI-S)

Some of the Microquartz fibers used in the processing of the General Electric samples were used in the "as-received" condition; some were given a special wash; and others were treated with silane prior to fabrication. Several types of proprietary binders were used on the samples studied. All forming was by vacuum casting from a slurry, followed by drying and firing. The fact that REI-S samples were received very early in the program indicates a pre-1972 fabrication.

Lockheed Missiles and Space Company (LI-1500)

All LI-1500 samples examined were made from Microquartz fibers. Specimens fabricated by Lockheed were received over the longest time span

of any of the types studied and, therefore, must be considered in terms of changing fiber purity and processing methods [TM X-2719, p. 2]. It has been previously noted that none of the LI-900 RSI currently baselined for the shuttle program were received and examined; therefore, all data and discussions are relevant to the older LI-1500 material.

Mullite

General Electric Company (REI-M)

Mullite tiles from General Electric were manufactured by vacuum casting, using several different types of binders. The tiles were formed, dried and fired in a manner similar, if not identical, to the process used by General Electric in the REI-S samples (TM X-2719, p. 34]. Some prefabrication processing was undertaken in the early work in order to reduce the amount of large agglomerates present in the initial lots of mullite fiber.

McDonnell-Douglas Astronautics Company (HCF)

The McDonnell-Douglas Astronautics Company added Eccospheres to the fiber and binder in order to reduce the density of the fired tiles. Eccospheres are thin-walled glassy spheres produced from fly-ash. During the development program, the contractor used several different binders.

COATINGS

In use, RSI will require a coating to water-proof the tile, provide optical properties to give the optimum dynamic thermal response and offer

a certain resistance to erosion during re-entry. The proper performance of these functions, together with the necessity that the coating be mechanically and chemically stable over the lifetime of the TPS requires that a number of properties be considered in the development of such coatings. These include:

1. Thermal emittance
2. Chemical and thermal expansion compatibility with RSI fibrous insulation
3. Water permeability
4. Mechanical strength
5. Thermal shock resistance
6. Thermal stability with respect to the properties listed above

The purpose of this study was primarily to determine the effects of thermal cycling upon the chemical and mechanical properties of the coatings. The particular aspects studied were the crystalline species present, degree of porosity, mechanical integrity (cracking, debonding, etc.), and dimensional stability.

The coating materials were, in general, glassy matrices containing various dispersed crystalline materials which were developed to achieve the desired properties. Because the details of the coating composition and structure were proprietary information, the coatings were characterized upon receipt. These analyses were accomplished by x-ray diffraction, x-ray spectroscopy, electron beam microprobe, scanning electron microscopy, and optical microscopy. In several instances, porosity was determined by mercury intrusion and water absorption.

General Electric

The General Electric coatings, designated Mod I and Mod IA, were glassy matrix materials containing nickel aluminate. Although the surface appeared porous, microscopic examination showed the crystalline material to be well sealed by the glass phase. The extreme difference between the mercury and the water porosity values indicated that the pore size was very small. The major difference observed in the two coatings was the lack of cristobalite in Mod IA.

McDonnell-Douglas

The McDonnell-Douglas HCF coatings, designated Mod I and Mod III, were complex layered structures comprised of a glassy layer next to the fiber insulation, an overlying layer of Cr_2O_3 in a glassy matrix, and a final, outer layer of a complex (Co, Fe, Cr) oxide. The major difference in the coatings was the presence of $AlPO_4$ in the Mod III coating.

Lockheed

The LI-1500 coatings were designated 0025 and 0042 so that a coated tile could be identified by a single number, e.g., 1525, which defined both the body of the tile and the coating. Both the 0025 and 0042 coatings were two-layer coatings. The layer adjacent to the fiber was glassy and dense; the second layer contained the crystalline thermal control compound, Cr_2O_3 or SiC, and was considerably more porous.

EXPERIMENTAL PROGRAM

TEST PROCEDURES

Quantitative Analysis by X-ray Diffraction

For the quantitative determination of α-quartz, α-cristobalite, and mullite, x-ray diffraction measurements were made with a Norelco x-ray diffractometer. Several methods of counting the intensity of the diffracted peaks were considered, but it was found that a simple ratio of the linear peak height of a sample to that of a standard was satisfactory. Absorption effects were ignored because the mass absorption coefficients of the vitreous and crystalline species were not significantly different in either the silica or the mullite samples.

The linearity of the x-ray diffraction peak heights was checked by preparing two sets of standards containing 20%, 40%, 60%, 80%, and 100% of each crystalline type. One set consisted of mixtures of cristobalite and quartz; the second set, of mullite and α-alumina. As a means of insuring accuracy, the intensities of the "100%" standards were checked at frequent intervals before and/or after a new group of samples was analyzed. A complete description of the procedures may be found in Appendix I of the Second Quarterly Progress Report (ref. 1).

Scanning Electron Microscope Examination

All samples of the fibers and tiles were examined by using a Cambridge Mark II Scanning Electron Microscope (SEM). Small amounts of the fiber

sample to be viewed were mounted on standard aluminum stubs by means of silver paint. After they had dried, these samples were coated in a vacuum evaporator, first with carbon and then with a 60% gold - 40% palladium alloy.

Tile samples which had been broken in tension were sectioned at the fracture surface, mounted, and prepared as described above. Other samples of the tiles were impregnated with methylmethacrylate, cured, cut, and polished (ref. 2). The polymethylmethacrylate (PMM) then was removed by heat treatment, and each sample was mounted and coated as already indicated.

Isothermal Heating

In order to compare the effects of isothermal heating, fiber specimens were placed in open platinum crucibles, and the tile specimens were palleted on pieces of like materials. Specimens were then heated in a resistance furnace according to the schedule given in table I. When appropriate, weights and dimensions were measured and recorded before and after heat treatments. Weight loss and crystalline content were determined for both fibers and tiles. Linear shrinkages were estimated for fibers and calculated for tiles.

Mercury Porosimetry

Pore size distributions of the tiles were studied by means of mercury porosimetry. This method consists of forcing a non-wetting liquid,

Table I.

Schedules Used in Isothermal Heating of Specimens

Temperature, K (°F)	Time, ks (hours)	
	Fiber	Tile
1255 (1800)	57.6 (16)	57.6 (16)
1365 (2000)	nm	1.8 (0.5)
	nm	7.2 (2)
	nm	57.6 (16)
1535 (2300)	1.8 (0.5)	1.8 (0.5)
	7.2 (2)	7.2 (2)
	57.6 (16)	57.6 (16)
1700 (2600)	1.8 (0.5)	1.8 (0.5)
	7.2 (2)	7.2 (2)
	57.6 (16)	57.6 (16)

mercury, into a porous body.

The minimum size pore which will be intruded by the mercury under a pressure P is given by the following equation:

$$D = \frac{-4\gamma \cos\theta}{P}$$

where: D = pore diameter

γ = surface tension of mercury

θ = wetting angle of mercury on solid in sample.

The volume of the pores was measured directly by observing the apparent decrease in the volume of mercury surrounding the specimen as pressure was increased. Thus, for each pressure there was a corresponding volume and minimum diameter of pores intruded. From the data, pore size versus pore volume distribution was determined. In addition, such quantities as porosity, bulk density, specific surface area, mean fiber diameter and volume, and linear shrinkage were determined for the specimens from these data.

Shrinkage and Expansion

Static shrinkage was determined by comparing the dimensions of specimens before and after heat treatment. Dynamic thermal expansion and shrinkage rates were measured on three 89 × 13 × 13 mm (3 1/2 × 1/2 × 1/2 in.) specimens in a resistance-heated thermal expansion furnace (ref. 3). Changes in length were measured by means of two telemicroscopes sighted on the ends of each specimen. The furnace was heated rapidly to the test temperature, and "point zero" was determined by a minor extrapolation of

shrinkage data. The analysis of the shrinkage as an activated process was completed by determining the shrinkage rates at two or more temperatures and then making an Arrhenius plot of log rate versus reciprocal absolute temperature. The slope of this plot should be $-E/R$, where E is the activation energy for viscous flow and R is the ideal gas constant.

Flight Simulation Thermal Cycling

For the purpose of simulating the effects of thermal cycling during re-entry, a radiant heat thermal-cycling test furnace was designed and constructed so that it would ramp to 1535 K (2300°F) in 300 seconds (five minutes). Constructed of insulating firebrick, the furnace enclosed a 100 × 100 × 75 mm (4 × 4 × 3 in.) cavity, with one open 100 × 100 mm (4 × 4 in.) face over which test specimens were placed. The furnace was heated by 4 silicon carbide heating elements. Figure 4 shows a typical heating-cycle curve. A 50 × 50 mm, a 75 × 75 mm, or a 100 × 100 mm (a 2 × 2 in., a 3 × 3 in., or a 4 × 4 in.) specimen could be placed in the door of the furnace. As desired, the heating of a specimen could be started at room temperature and continued on a given schedule, or the furnace could be heated to a predetermined temperature and a specimen then placed in position. A spring-loaded thermocouple measured the front-face temperature of the specimen, and a thermocouple in the center of the cavity was used for control.

After being cycled ten times at 1365 or 1535 K (2000 or 2300°F), the specimens were cut in half. One section was trimmed to remove the selvage which had not been exposed to the direct heat of the heating

elements. Successive layers (about 0.3 mm [0.012 in.] thick) were removed with a microtome, beginning with the front (hot) face and continuing toward the rear (cold) face. Then x-ray diffraction analyses were made on a sample from each layer.

Coatings

Three specimens of each of the RSI coatings tested were cut from tiles provided by the contractors so that the coating would remain intact with respect to the tile. In each case, two specimens were subjected to thermal treatment, one undergoing a maximum hot-face temperature of 1365 K (2000°F) and the other, a maximum hot-face temperature of 1535 K (2300°F); the third specimen was reserved. The cycling was conducted as follows. With the coating face inward, a specimen was placed in a window of a furnace which had been heated to a temperature of 1090 K (1500°F); the furnace's temperature was raised in less than sixty seconds to the maximum temperature and held there for 900 seconds (15 minutes); then the furnace's power was cut off. After the furnace and specimen had been allowed to cool to 1090 K (1500°F), the specimen was taken from the furnace to ambient air; another specimen was put in its place; and the cycle was repeated. The cycling was normally done with pairs of specimens.

Samples were then cut from the specimens for examination by x-ray diffraction, electron microprobe, SEM, and optical microscope, and, in some cases, samples were obtained for x-ray spectrographic analysis and porosity determinations. The general method for examination of coating cross sections was to infiltrate the specimen with methyl methacrylate,

polymerize to polymethylmethacrylate (PMM), section, and polish. The PMM was then removed by heating each sample at 810 K (1000°F). For samples of the MDAC MOD III coating, this treatment resulted in loss of the outer layer of the complex coating, but these effects were recognized and accounted for.

Porosity data were obtained by two methods, water absorption and mercury intrusion. The procedure for determining water absorption was to immerse a weighed sample of coating in boiling water for 86.4 ksecs (24 hrs.). The sample was then weighed in air and reweighed while suspended in water. From these data and from the original weight, the porosity that was filled during immersion was calculated. The mercury intrusion data were obtained by using a mercury porosimeter capable of intruding mercury into a 12 nm pore. Thus, in any discussion of these data, it must be remembered that water can penetrate open porosity as small as 0.15 nm (1.5Å), while the mercury data only shows open porosity that is 12 nm (120Å), or larger.

Mechanical Properties

Tensile strengths were measured on segments cut from the tiles. T-shaped aluminum grips were cemented with epoxy resin to the two opposing faces. In most cases, the dimensions of the segments were 25 × 25 × 13 mm (1 × 1 × 1/2 in.) and the grips were cemented to the 25 × 13 mm (1 × 1/2 in.) faces. In cases in which prolonged heat treatment had produced substantial shrinkage, the longer dimensions of the segments were less than one inch.

The tensile test was made on a Model TT-CM Instron Universal Testing Machine, using a crosshead speed of 1.7 μm/sec (0.01 cm/min). Strain

measurements were obtained from an extensometer which was connected to the T-grips at the specimen, and load-extension was plotted directly on the standard Instron x-y recorder.

Two testing directions were adopted. The first was tensile loading parallel to one of the long dimensions of the tile (designated as parallel to the x-y plane), and the second was tensile loading parallel to the short tile dimension (designated as parallel to the z-direction). The directional orientation of the test specimens relative to the parent tile was carefully maintained.

Specimens were tested in the "as-received" condition and after the different isothermal heat treatments described above. The density of the test specimens was obtained from their weight and the external dimensions, and the crystalline content was measured as indicated in the section on "Quantitative Analysis by X-ray Diffraction."

RESULTS

Devitrification/Crystallization

Although the "as-received" fibers were primarily vitreous or non-crystalline, it was known that heat would cause either devitrification or crystallization. Moreover, it seemed clear that the processing of the tiles could affect the devitrification/crystallization characteristics of the fibers which they contained, as well as of the binders and/or other additives. The results of investigating these aspects of RSI follow, organized essentially by fiber type.

"As-Received Fibers"

Silica. In the temperature range of interest in this work (up to 1700 K [2600°F]), glass is a metastable form of silica. The glass therefore can convert to a more stable crystalline form if it is held at appropriate temperatures for a sufficient period of time. A schematic diagram of the stable and metastable forms of silica is shown in figure 5. Although the results of numerous studies on the devitrification of vitreous silica have been published, most of that work was accomplished by using bulk specimens. Thus, the high surface area of the fibers involved in this study adds a further dimension to earlier work. The scope of this project did not permit a quantitative study of fiber devitrification kinetics from a theoretical standpoint. Therefore, the concepts suggested here must be considered as being empirical.

In general, the devitrification of a glass is nucleated at a surface and proceeds inward. The ease with which the phase transformation is initiated is highly dependent on surface condition, impurities, and the particular crystalline modification which first appears. The growth rate of the nucleated phase depends on the degree of undercooling for that particular phase and the mobility of the atomic groups which rearrange themselves.

The determination of reproducibility of analyses for crystalline content was made on samples from Lot 2102. For this purpose, 1/2 gram specimens were isothermally heated to 1535 K (2300°F) in open platinum crucibles for periods of 1.8, 7.2, and 57.6 ks (1/2, 2, and 16 hrs.). Four tests were run at 1.8 ks (1/2 hr.); three, at 7.2 ks (2 hrs.); and two, 57.6 ks (16 hrs.). The specimens were all heated in the same furnace and were analyzed by two different operators over a period of three months. The results as shown in table II indicate a maximum error of ± 9% at a 95% confidence level and also show that ten or more specimens must be run in order to estimate the crystallinity to within ± 2%.

Of a total of nineteen lots of Microquartz fibers received, devitrification studies were made upon ten. The results of experiments at 1255, 1535, and 1700 K (1800, 2300, and 2600°F) are given in table III. None had any crystalline material present in the "as-received" state. A wide variability was observed in the devitrification behavior of the different silica materials, and sometimes within different samples of the same lot of material. As a consequence of these observations, the following generalizations may be made.

Table II.

Reproducibility of Quantitative Analyses for
Devitrification Products in Lot 2102 Microquartz Fiber
When Isothermally Heated to 1535 K (2300°F)

Devitrification Product	Weight Percent Devitrification Product		
	ks (hours) at Temperature		
	1.8 (0.5)	7.2 (2)	57.6 (16)
Cristobalite	13	32	65
	11	38	69
	11	45	nm
	5	nm	nm
	10.0*	38.5*	67.0*
Quartz	72	38	19
	68	37	16
	67	48	nm
	53	nm	nm
	65.0*	41.0*	17.0*
95% Confidence Interval	± 6	± 7	± 9

*Mean

Table III.
Effect of Isothermal Heating upon Devitrification of Microquartz Fibers

Lot Identification	Source	Devitrification Product	Isothermal Heating Temperature						
			1255 K (1800°F)	1535 K (2300°F)			1700 K (2600°F)		
			Time - ks (hrs.)						
			57.6 (16)	1.8 (0.5)	7.2 (2)	57.6 (16)	1.8 (0.5)	7.2 (2)	57.6 (16)
			Weight Percent Devitrification Product						
1437	LMSC	Cristobalite	0	51	50	56	95	nm	100
		Quartz	6	38	24	18	0	nm	0
1466	LMSC	Cristobalite	65	91	96	91	89	nm	100
		Quartz	0	0	0	0	0	0	0
1986	ARC	Cristobalite	0	23	64	77	88	93	100
		Quartz	0	2	0	0	0	0	0
Unknown (Untreated)	GE	Cristobalite	0	50	66	62	72	nm	96
		Quartz	10	0	0	0		nm	0
Unknown (Silane Treated)	GE	Cristobalite	Tr	33	59	56	59	nm	84
		Quartz	10	63	18	16	Tr	nm	0
Unknown	ARC	Cristobalite	9	62	69	74	9	nm	95
		Quartz	22	5	7	Tr	0	nm	0
2083	LMSC	Cristobalite	0	0	0	21	0	nm	95
		Quartz	0	0	0	0	0	0	0
2102	ARC	Cristobalite	Tr	5	32	65	69	nm	86
		Quartz	0	53	38	19	0	nm	0
2148	ARC	Cristobalite	0	2	2	5	13	77	100
		Quartz	0	0	1	0	0	0	0
2155	ARC	Cristobalite	0	0	2	13	23	nm	100
		Quartz	0	0	0	2	0	nm	0
2273	ARC	Cristobalite	0	0	0	9	Tr	36	100
		Quartz	0	0	0	0	0	0	0

In those cases in which little devitrification occurred after an extended time at high temperatures, nucleation rather than growth rate was probably controlling. Growth rates are generally considered to be linear with time, but, in several cases, the increase in crystalline content was greater than expected by factors of four to eight.

At 1255 K (1800°F) quartz is the stable crystalline phase. This phase was observed in all except for the specimens from Lot 1455 and the Ames "unknown" (which contained 65% and 9% cristobalite, respectively) after 57.6 ks (16 hrs.) at 1255 K (1800°F). These two cases are examples of metastable phase growth.

Other examples of metastable growth occurred during the 1535 K (2300°F) heating. At this temperature, cristobalite is the stable phase, while quartz is the metastable phase. Quartz was observed as the initial devitrification product and then decreased in concentration as the transformation to cristobalite occurred. The appearance of quartz is probably nucleation controlled. There were indications in short-time heating tests that cristobalite formation is linked to the quartz precursor, because the initial formation of cristobalite did not start until after the quartz had formed. As the amount of cristobalite increased, the concentration of quartz decreased. These results can be observed in table III.

At 1700 K (2600°F) cristobalite is the stable phase, and the free energy of quartz is higher than the free energy of the vitreous state. The melting point of metastable quartz is estimated to be 1670 K (2550°F); thus, cristobalite would be expected as the only devitrification product present above this temperature. This was confirmed by the data.

The use of a mobility factor for predicting devitrification characteristics as a function of impurity levels depends upon the availability of meaningful analyses of impurity content. The coefficients given in the quarterly reports were based upon spectrochemical analyses of samples from six lots of Microquartz. Use of an inverse matrix resulted in what appeared to be meaningful coefficients. However, subsequent atomic absorption analyses of these samples and samples from several other lots made possible the substitution of additional data within the matrix, and these resulted in unrelated coefficients. It is therefore apparent that additional impurities, cross-correlations of impurities, and factors other than composition must be considered as contributing to devitrification.

Mullite. The fabrication of mullite fibers is entirely different from that used in the production of silica fibers, and the result of heat treatment is one of crystallization rather than devitrification. Because crystallization proceeded at a consistently rapid rate and because no phase transformations exist between room temperature and the incongruent melting temperature of mullite, the effect of temperature on mullite fibers received less attention.

"As-received" samples of mullite fiber contained some crystalline mullite and γ-Al_2O_3. Aluminum borate ($AlBO_3$) was observed in three of the earlier lots. The results of heat treatment upon mullite crystallization are given in table IV.

Table IV.
Effect of Isothermal Heating upon Crystallization of Mullite Fibers

Lot Identification	Source	"As-Received"	Isothermal Heating Temperature						
			1255 K (1800°F)	1535 K (2300°F)			1700 K (2600°F)		
			Time - ks (hrs.)						
			57.6 (16)	1.8 (0.5)	7.2 (2)	57.6 (16)	1.8 (0.5)	7.2 (2)	57.6 (16)
		Weight Percent Mullite							
Old (6/70)	MDAC	19	nm	nm	66	65	70	89	94
New (11/70)	MDAC	14	nm	nm	78	84	88	96	96
New (5/71)	NDAC	11	19	36	78	77	91	92	100
S-98-E	GE	12	26	76	87	94	93	96	100
S-98-F	GE	18	nm	nm	nm	nm	nm	nm	nm
Old	GE	19	nm	nm	nm	87	91	91	86
Scrap	GE	15	19	nm	73	nm	88	nm	nm

Processed Tile

Silica. The results of the analyses for crystalline content in processed tile are given in tables V and VI. Those listed in table V were analyzed in the "as-received" condition only. From them it is apparent that improvements in fiber, binder, and processing materially reduced the residual crystalline content of later tiles. Isothermal heating of samples resulted in the data shown in table VI. Unfortunately, samples from the fiber lots used to fabricate these tiles were not provided so the effects of heating fibers and tiles could not be compared directly. Without this comparison, only the following assumptions can be made.

TT-14-B was fabricated from a fiber lot similar to that of Lot 1986 or Lot 2102. If it was similar to that of 1986, the increase in quartz found in the 1535 K (2300°F) heat treatment would be due to devitrification of the binder. If the original fiber was similar to that of 2102, the decrease in quartz at 1535 K (2300°F) and the increase in cristobalite would be due to heating the tile during processing. Similar generalizations may be drawn by assuming that TT-48-3 was made from Lot 2083; TT-399-6, from Lot 2273; and AIM 301-1, from Lot 2083.

A specimen from LI-1525 was subjected to five cycles of isothermal heating to 1535 K (2300°F) for one hour and a return to room temperature. X-ray analysis showed the following:

Crystalline Content	One Cycle	Five Cycles
Cristobalite (wt %)	13	60
Quartz (wt %)	15	7

Table V.

"As-Received" Crystalline Content of Several Silica Tiles

Sample Identification	Source	Crystalline Phases Present	Crystalline Content (Weight Percent)
REI-Silica 8/71	GE	Cristobalite Quartz	41 0
LI-1500 1970 tile	LMSC	Cristobalite Quartz	9 29
MSC-0361	LMSC	Cristobalite Quartz	0 14
774	LMSC	Cristobalite Quartz	0 6
X-887	LMSC	Cristobalite Quartz	0 0
AIM 301-2	ARC	Cristobalite Quartz	0
301-3	ARC	Cristobalite Quartz	0 0
301-4	ARC	Cristobalite Quartz	0 0

Table VI.
Effect of Isothermal Heating upon Crystalline Content of Silica Tile

Sample Identification	Source	Devitrification Product	"As-Received"	Isothermal Heating Temperature								
				1365 K (2000°F)			1535 K (2300°F)			1700 K (2600°F)		
				Time - ks (hrs.)								
				1.8 (0.5)	7.2 (2)	57.6 (16)	1.8 (0.5)	7.2 (2)	57.6 (16)	1.8 (0.5)	7.2 (2)	57.6 (16)
			Weight Percent Crystalline Content									
LI-1525 (TT-14-B)	LMSC	Cristobalite	4	0	0	6	13	55	61	85	89	95
		Quartz	5	4	4	5	19	15	5	0	0	0
LI-1542 (TT-48-3)	LMSC	Cristobalite	0	0	0	0	0	0	4	0	5	96
		Quartz	0	0	0	0	0	0	0	0	0	0
LI-1542 (TT-70-2)	LMSC	Cristobalite	0	na	na	na	0	0	3	na	na	na
		Quartz	0	na	na	na	0	0	0	na	na	na
LI-1542 (TT-139-6)	LMSC	Cristobalite	0	0	0	0	0	0	81	0	38	100
		Quartz	0	0	0	0	0	0	0	0	0	0
AIM (301-1)	ARC	Cristobalite	Tr	0	0	0	1	2	90	4	90	100
		Quartz	0	0	0	0	0	0	0	0	0	0

These data indicate that the single cycle treatment was equivalent to 1.8 ks (1/2 hr.) of isothermal heating and that the crystalline content at the close of five cycles was similar to the result obtained after 57.6 ks (16 hrs.) of isothermal heating.

Thermal cycling tests were run on a specimen from LI 1500 x-847C in order to determine the effective depth of devitrification. The specimen was completely vitreous in the "as-received" state. The data (fig. 6) show that after twenty cycles, the depth of devitrification was less than 5 mm (0.2 in.). Such a result suggests that any effects of strength degradation caused by low temperature phase transitions will be restricted to the surface of the tile.

Mullite. The results of x-ray diffraction analyses of processed mullite tiles are given in table VII. These make it apparent that contractor processing developed the majority of the mullite in the tile. The high cristobalite content of the MDAC Phase I was undoubtedly due to the devitrification of the ECCO spheres. Table VIII shows the effect of isothermal heating on several tile samples. The reduction of cristobalite content to zero in the MDAC Mod I and III can be accounted for by the remelting of these spheres. The presence of smaller quantities of cristobalite in the MDAC Mod III and the GE-REI-M samples was probably due to the types of binder employed.

Morphology

Morphological studies resulted in data on the size and size distribution of the fibers in the "as-received" lots and in the tiles, a

Table VII.

"As-Received" Crystalline Content of Several Mullite Tiles

Sample Identification	Source	Crystallization Product	
		Composition	Weight Percent
HCF	MDAC	Mullite	32
Old Binder #1	MDAC	Cristobalite	13
Old Binder #2	MDAC	Mullite	35
		Cristobalite	13
Old Binder #3	MDAC	Mullite	28
		Cristobalite	19
New Binder #1	MDAC	Mullite	30
		Cristobalite	17
New Binder #2	MDAC	Mullite	38
		Cristobalite	14
Phase I (31 T-1)	MDAC	Mullite	36
		Cristobalite	36
REI - 1970	GE	Mullite	100
JG - 52	GE	Mullite	71
JG - 53	GE	Mullite	71

Table VIII.

Effect of Isothermal Heating upon Crystalline Content of Mullite Tile

Sample Identification	Source	Crystallization Product	"As-Received"	Isothermal Heating Temperature											
				1365 K (2000°F)			1535 K (2300°F)			1700 K (2600°F)					
				Time - ks (hrs.)											
				1.8 (0.5)	7.2 (2)	57.6 (16)	1.8 (0.5)	7.2 (2)	57.6 (16)	1.8 (0.5)	7.2 (2)	57.6 (16)
			Weight Percent Crystalline Content												
HCF MOD I	MDAC	Mullite	56	54	51	53	52	47	47	55	52	46
		Cristobalite	12	13	12	12	3	8	0	0	0	0
MOD III (C-31-4)	MDAC	Mullite	70	62	65	60	65	65	65	60	60	83
		Cristobalite	8	6	1	0	1	3	3	0	0	0
REI-MOD I (11-4)	GE	Mullite	50	79	77	77	73	74	77	79	75	75
		Cristobalite	7	5	5	6	5	6	6	1	2	1
MOD-IA (ML-49)	GE	Mullite	77	79	74	66	79	82	75	86	90	77
		Cristobalite	5	2	4	7	0	1	0	1	1	1
MOD-IA (ML-122)	GF	Mullite	74	70	81	79	80	82	73	89	81	79
		Cristobalite	4	3	3	7	3	3	9	1	0	1

comparison of their characteristics before and after heat treatment, and the effectiveness of the fiber-to-fiber binding in the tiles. Evaluations were based upon studies of SEM photographs.

"As-Received" Fibers

Silica. SEM examination of the "as-received" lots indicated that the majority had fibers of consistent size. However, samples from a few lots had a considerable variation, with a tendency towards small diameter fibers. Two photographs were taken of later fiber lots, and thirty-five diameters were measured to the nearest 0.1 mm on each photograph in order to obtain the size distribution. The surface areas per gram were calculated after dividing fiber diameters into seven or eight bands of equal width on a log scale. Each successive cell was twice the preceding one on a linear scale. The results are given in table IX. The extremes of these data for finer than 0.8 μm are 8.6% for Lot 2155 and 23.9% for Lot 1986. The calculated surface areas agree reasonably well with the values obtained by nitrogen adsorption, except for Lot 2155, in which the difference is quite large. The data indicate that the fibers, except in Lot 2155, are probably pore-free to nitrogen adsorption. Further work in this area is needed.

Size ranges in silica fibers become important in two significant areas. First, a large percentage of small diameter fibers will cause considerable softening and loss of structure at high temperatures, as will be seen in a following section. Second, the maximum photon scattering efficiency is attained with 1 μm diameter fibers. If too many fibers in excess of 3 μm are present, the insulative properties of a material will be significantly reduced.

Table IX.

Distribution of Fiber Diameters as Measured on Several Lots of Microquartz

Fiber Diameter (μm)	Cumulative Percent Finer than Stated Size					
	Fiber Lot 2083	2102	2155	2158	1986	2273
0.1	4.3	1.5	0.0	4.3	4.5	1.4
0.2	10.0	4.5	2.9	11.4	14.9	5.7
0.4	18.6	19.2	8.6	18.6	23.9	18.6
0.8	45.7	30.9	25.7	42.9	38.8	42.9
1.6	57.1	70.6	55.8	55.7	64.2	72.9
3.2	97.2	97.1	77.2	91.5	89.6	95.6
6.4	100.0	100.0	100.0	100.0	100.0	100.0
Surface Area ($m^2/kg \times 10^{-3}$)						
Calculated	3.78	2.77	1.91	3.57	3.95	3.04
Measured (by N_2 adsorption)	3.6	2.4	5.5	3.2	3.0	nm

Mullite. The most obvious characteristics of the early "as-received" mullite lots were the relatively large fibers and wide range of fiber diameters, as well as the presence of agglomerated fiber or "shot." In later lots, the range of fiber diameter and agglomeration were either reduced or eliminated.

Fibers after Heat Treatment

Silica. The effect of a substantial number of very small diameter fibers upon softening at 1255 K (1800°F) is shown in figures 7a and 7b. Exposure to an even higher temperature (1700 K [2600°F]) resulted in a substantial loss of fiber shape in all of the silica fibers examined (fig. 7c). Obviously, in addition to the distribution of fiber diameters, the types and concentration of impurity also make a substantial contribution to these effects.

The silica fibers were non-crystalline in the "as-received" state and SEM examination showed little or no surface effects (fig. 8a). After heat treatment, the morphology of the fibers was affected by devitrification as shown in figure 8b. Figures 8c and 8d show the post-heat treated fiber structure after etching with hydroflouric acid.

Mullite. Deformation at higher temperatures was seldom observed in the more refractory mullite fibers (fig. 9). The primary temperature effect was crystallization. The small, needle-like mullite fibers observed on the surface in high magnification SEM photographs (fig. 10a) and on fracture surfaces (fig. 10b) indicated a general distribution of the crystalline material throughout the fiber.

"As-Received" Tiles

SEM photos of the early tiles showed considerable fiber orientation due to processing (ref. 4). Also, the use of different experimental binders by contractors resulted in extensive differences in the morphology as observed in SEM photos. A greater consistency developed in both of these areas as improvements were made; consequently, details of the morphology of early tiles will not be discussed here.

Bonding in Silica. The bonding in silica tiles was primarily due to a glassy fillet, although the amount observed varied from tile to tile. Figures 11 and 12 show the nature of the bonding in several LI-1500 specimens at different magnifications. Figure 13 shows the bonding in AIM tile to be present in lesser amounts than in the Lockheed samples.

Bonding in Mullite. The crystalline nature of the fired mullite fiber presented an entirely different bonding problem in the processing of the tiles. Examinations of bonds from various samples showed some glass bonds (fig. 14), crystalline bonds (fig. 15), and glass-crystalline bonds (fig. 16). MDAC's use of Eccospheres resulted in the development of a siliceous bond as some of these spheres or their fragments softened during processing (fig. 17).

Porosity

Mercury porosimetry provided data on pore volume, on porosity of the tiles, and for calculating bulk density (ρ_b). The values obtained, plus the values of bulk densities derived from direct measurements, are given in table X. The pore size distribution varied by fiber type and by manufacturer. The silica tile from Lockheed appeared to have a log-normal

Table X.

Comparison of Data Obtained by Mercury Porosimetry on "As-Received" RSI Tiles

Tile Identification	Source	Pore Size Distribution	Pore Volume m^3/kg (cc/g)	Porosity (%)	Bulk Density - kg/m^3 (lbs/ft^3)	
					Porosimetry	Direct Measurement
LI-1542	LMSC	Log-Normal $\overline{D}_p$ = 16 µm	3.5×10^{-3} (3.5)	89.1	255.2 (15.9)	259.5 (16.2)
MOD I	MDAC	Complex $\overline{D}_p$ = 86 µm	2.6×10^{-3} (2.6)	89.1	342.8 (21.4)	277.1 (17.3)
MOD III	MDAC	Complex $\overline{D}_p$ = 65 µm	3.0×10^{-3} (3.0)	90.4	301.1 (18.8)	297.9 (18.6)
MOD IA	GE	Normal $\overline{D}_p$ = 91 µm	4.3×10^{-3} (4.3)	93.2	216.2 (13.5)	200.2 (12.5)

distribution of pore size with a mean diameter of 16 μm. The mullite tile of General Electric showed a normal distribution with a mean diameter of 23 μm. The MDAC tile had a complex distribution of pore sizes, deviating from a normal distribution at both ends of the curve.

The total open pore volume was measured directly. Then, consideration of the nature of the tile led to the assumption that there were no closed pores and that, consequently, density could be determined from the data on volume. The pore size and distribution information derived from these measurements could be useful in the calculation of theoretical heat transfer values.

Shrinkage

All shrinkage measurements were made in the x- or y-directions because none of the tile specimens received were of sufficient thickness to obtain a z-direction sample. Most of the specimens tested exhibited nearly constant shrinkage rates over the range of temperatures used. Table XI shows the results of curve-fitting the data to a least-squares straight line, and the high values of correlation coefficients attest to an appropriate fit. The total shrinkage of the tile specimens tested was generally less than 10%.

Figure 18 presents Arrhenius plots of the data. The activation energies for the shrinkage of each tile in the x-y plane were determined from the slopes of these curves. The values thus derived agree with values from viscosity-versus-temperature curves for vitreous silica (ref. 5) and with values reported by Hetherington, et al. (ref. 6). The use of these data will be discussed further under the section on modeling.

Table XI.

Shrinkage Rates Determined for Three Silica Tiles

Tile Number	Specimen Number	Temperature K (°F)	Shrinkage Rate (%/hr.)	Correlation Coefficient
LI-1542 (TT 139-6)	E-1	1523 (2287)	0.9911	+ 0.99912
	E-3	1551 (2338)	2.2481	+ 0.99989
	E-4	1577 (2385)	4.7614	+ 0.99982
LI-1542 (TT 70-2)	B-2	1523 (2287)	1.0610	+ 0.99998
	B-2	1560 (2354)	3.0917	+ 0 99980
AIM 301-3	1	1523 (2287)	1.7496	+ 0.99916
	1	1556 (2347)	4.3050	+ 0.99857
	2	1543 (2327)	3.3202	+ 0.99941

Linear and bulk shrinkage values were calculated from mercury porosimetry data (ref. 7). Typical results are shown in the last two columns of table XII.

Mechanical Properties

The mechanical property testing resulted in data on the comparative strengths of (a) the different kinds of tile (silica and mullite), (b) the same type of tile from different manufacturers, and (c) different lots of the same tile from the same manufacturer. In addition, it provided data on the effect which heat treatment had on strength.

The tensile strengths of the processed tiles were highly anisotropic, generally being greater by a factor of three or four in the x - y (in-plane) direction than in the z (perpendicular) direction. This difference is obviously related to the structural anisotropy resulting from processing of the tile. The average strength of all "as-received" tile types was between 340 to 690 kN/m^2 (50 and 100 psi), except for one early version of the General Electric mullite, the strength of which was less than 170 kN/m^2 (25 psi).

The effect of heat treatment on the strength of silica tile was significant. The influence on strength of cristobalite, the primary devitrification product, becomes apparent upon examination of figure 19, which shows the thermal expansion of vitreous silica, quartz, and cristobalite. The low to high inversion of cristobalite at 470 K (200°F) is reversible and is accompanied by a large change in volume. The strength of fibers with a significant cristobalite content can be expected to degenerate during low-temperature thermal cycling.

Table XII.

Linear and Bulk Shrinkage of RSI Tile
as Determined by Mercury Porosimetry

Identification	Source	Heat Treatment	Bulk Density kg/m^3 (lbs/ft^3)	Shrinkage (%) Volume	Linear
LI-1542	LMSC	None ("As-Received)	255.2 (15.9)	nm nm	nm nm
		1530 K (2300°F) (2 hrs.)	382.7 (23.9)	33.1	12.5
		1530 K (2300°F) (16 hrs.)	816.9 (51.0)	68.7	32.1
MOD I	MDAC	As Received	342.8 (21.4)	nm nm	nm nm
		1700 K (2600°F) (16 hrs.)	369.8 (23.1)	6.9	2.4
		1700 K (2600°F) (64 hrs.)	553.1 (34.5)	37.7	14.6
MOD III	MDAC	As Received	301.1 (18.8)	nm nm	nm nm
		1700 K (2600°F) (16 hrs.)	321.6 (20.1)	6.0	2.0
		1700 K (2600°F) (64 hrs.)	311.9 (19.5)	3.0	1.0
MOD IA	GE	As Received	216.2 (13.5)	nm nm	nm nm
		1700 K (2600°F) (16 hrs.)	199.4 (12.5)	- 8.7	- 3.0
		1700 K (2600°F) (64 hrs.)	249.2 (15.6)	13.0	4.5

A series of cube specimens, 25 mm (1 in.) on an edge, were cut from "as-received" AIM tiles 301-2, 301-3, and 301-4, which had zero cristobalite content present. The specimens were heat-treated at 1644 K (2500°F) to yield various levels of cristobalite content. The tensile strengths were measured and density effects were normalized to 250 kg/m^3 (15 lbs/ft^3) by multiplying the measured strength by $(250/\rho_b)$, where ρ_b was the measured bulk density of the heat treated specimens in kg/m^3. (See equation 6, on page 51.) The results are given in table XIII and the data points are plotted in figure 20.

A significant degradation of strength occurred with the formation of cristobalite. Only 0.3 weight fraction cristobalite reduced tensile strength to nearly one-half of its value in "as-received" tile, and 0.65 weight fraction cristobalite reduced tensile strength to one-sixth of the "as-received", value.

Samples containing the four lowest levels of cristobalite were thermally cycled ten times through the α - β cristobalite inversion temperature, but only relatively small decreases in strength were observed, amounting to not more than 15% of the predicted strength. The dashed line in figure 20 represents the worst probable case -- minimum strengths after severe thermal cycling of the partially devitrified tiles. If this representation is accurate, a tile with a cristobalite content of 15% might be expected to lose 20% of its strength after ten low temperature cycles. The solid line in figure 20 will be discussed in the section on modeling.

The later silica materials, LI-1542 and AIM 301-1, did not devitrify appreciably at 1535 K (2300°F) heat treatment. Although there was an

Table XIII.

Effects of Cristobalite Content on Tensile Strength of AIM Silica RSI Normalized to 250 kg/m^3 (15 lbs/ft^3)

Specimen Number	Average Cristobalite Content (%)	Normalized Tensile Strength N/m^2 (psi) 301-2	301-3	301-4	Average Strength
"As-Received"	0	- -	- -	- -	421 (61)
1	21	269 (39)	172 (25)	290 (42)	244 (35)
2	65	131 (19)	39 (6)	21 (3)	163 (9)
3	29	255 (37)	221 (32)	228 (33)	234 (34)
4	40	172 (25)	241 (35)	276 (40)	228 (33)
5	48	214 (31)	296 (43)	290 (42)	267 (39)
6	85	21 (3)	4 (1)	28 (4)	17 (3)
7	17	283 (41)	324 (47)	283 (41)	297 (43)
8	6	331 (48)	352 (51)	393 (57)	359 (52)
9	13	386 (56)	303 (44)	296 (43)	331 (48)
10	28	269 (39)	276 (40)	269 (39)	269 (39)

apparent increase in strength, only a slight change was observed when the values were corrected for density (fig. 21).

The mullite tiles also showed little changes in strength due to similar heat treatments (fig. 22).

Coatings

The test program for coatings produced data on the effect which thermal cycling had on their chemical and morphological properties. Six coatings were studied: Lockheed 0025 and 0042, General Electric Mod I and Mod IA, and McDonnell-Douglas Mod I and Mod III. Each of the coatings was subjected to 10 cycles of heating to each of two temperatures, 1360 K and 1520 K (2012°F and 2282°F).

Lockheed LI-1500 Coatings

The x-ray diffraction analysis of the Lockheed 0025 and 0042 coatings showed that the only effect of the heat treatment due to thermal cycling was devitrification to cristobalite in the glass phase. The results are summarized below:

Specimen	"As-Received"	10 cycles 1370 K (2012°F)	10 cycles 1530 K (2282°F)
LI-0025	glass, Cr_2O_3	≈ 15% cristobalite, Cr_2O_3	≈ 25% cristobalite, Cr_2O_3
LI-0042	α - SiC	≈ 3% cristobalite, SiC	≈ 8% cristobalite, α - SiC

SEM examination of both "as-received" coatings showed considerable porosity in the outer layer, but a well-sealed intermediate layer. The 0042 coating was the only one examined after thermal cycling. After 10 cycles at 1520 K (2282°F), the intermediate glass layer showed extreme porosity, with apparent growth of the layer. The increased porosity resulted in an increase in the coating's thickness of as much as 100%. Figures 23a and 23b compare optical thin sections of this coating in the "as-received" condition and after 10 cycles of heating to 1520 K (2282°F). The water absorption and mercury porosimetry data as shown below are in accord with the results of the microscopy.

Thermal Treatment	Porosity, % H_2O Absorption	Porosity, % Hg Intrusion
"As-Received"	11.3	13.8
10 cycles, 1360 K (2012°F)	14.3	14.3
10 cycles, 1530 K (2232°F)	24.7	29.7

The porosity data may not indicate the absolute pore volume because much of the porosity appears to be closed and thus would not be detected by the method used.

General Electric REI Coatings

When subjected to 10 cycles of heating to 1520 K (2282°F), the Mod I coating showed a gross penetration of the glassy phase into the underlying tile. The penetration was very noticeable because the glassy phase was colored green due to the presence of nickel. The Mod IA coating exhibited none of this behavior.

The effect of thermal cycling upon the crystalline content of the Mod I and Mod IA coatings is shown below:

Specimen	"As-Received"	10 cycles 1370 K (2012°F)	10 cycles 1250 K (2282°F)
Mod I	mullite 5% cristobalite nickel aluminate	no change	cristobalite increased to 15%
Mod IA	mullite nickel aluminate trace of cristobalite	no change	no change

Porosity data were not obtained for the Mod I coating. However, as measured by mercury intrusion and water absorption in the "as-received" and heat-treated specimens, the porosity of the Mod IA coating was found to be as follows:

Thermal	Porosity, % H_2O Absorption	Porosity, % Hg Intrusion
"As-Received:	19.4	4.3
10 cycles, 1370 K (2012°F)	16.6	4.6
10 cycles, 1520 K (2282°F)	18.2	4.5

The data show essentially no difference in porosity between the heated specimens and the "as-received" coating. The large difference between the porosity values measured by water absorption and those measured by mercury intrusion indicates that approximately 80% of the porosity was smaller than 15 μm.

McDonnell-Douglas HCF Coatings

As the results shown below indicate, x-ray diffraction studies revealed that thermal cycling had little effect on the crystalline species present in the Mod I and III coatings:

Specimen	"As-Received"	10 cycles 1370 K (2012°F)	10 cycles 1520 K (2282°F)
Mod I	cristobalite, quartz, Cr_2O_3 $(Co, Cr, Fe)O_3$	no change	no change
Mod III	same as Mod I	no change	no new phases, slight increase in cristobalite content

SEM examination of the Mod I coating after cycled to 1520 K (2282°F) indicated the presence of a new dendritic phase at the interface between the outer layer containing $(Co, Fe, Cr)O_x$ and the intermediate layer composed of Cr_2O_3 in a glassy matrix (fig. 24). Electron microprobe examination showed the migration of cobalt and iron into and beyond this region; the chromium, however, did not appear to diffuse under these conditions. The Mod I coating showed no indication of the new phase or of cobalt and iron migration.

SEM examination of cross sections of the Mod III coating after cycling to 1520 K (2700°F) showed a dramatic increase in porosity as compared with the "as-received" specimen (figs. 25a and b). Suspecting that sample preparation might have had some effect on this, fracture surfaces of this same specimen were examined and found to have a similar porosity. On the other hand, the porosity of this coating, as measured by water absorption and mercury porosimetry, showed essentially no increase as a result of the

thermal treatment. The inconsistency of this result and the SEM data remains unexplained.

Thermal Treatment	Porosity, % H_2O Absorption	Porosity, % Hg Intrusion
"As-Received"	25.4	21.1
10 cycles, 1370 K (2000°F)	24.3	18.1
10 cycles, 1520 K (2700°F)	28.0	15.5

MODELING

STRENGTH OF INDIVIDUAL FIBERS

A structural model was developed to explain the strength in RSI silica tiles. This model consists of layers of silica fibers of uniform diameter D and separation L, with each successive layer being rotated ninety degrees with respect to the preceding layer. For obvious reasons this has been termed the "Stack-of-Logs" model (ref. 9).

The bulk density is determined by considering a volume with the dimensions $D \times L \times L$. Within this bulk volume is contained one equivalent fiber with the volume $\frac{\pi D^2}{4} L$. Thus, bulk density can be determined from the following equation:

$$\rho_b = \frac{\pi}{4} \frac{D}{L} \rho_t \tag{1}$$

where: ρ_t is the true density of the fibers.

Since ρ_b and ρ_t are measureable, D/L can be determined and employed to describe the mechanical properties of the structure:

$$(D/L) = \frac{4}{\pi} \frac{\rho_b}{\rho_t} \tag{2}$$

Mechanical properties in the symmetrical $x-y$ plane may be predicted from this model on the assumption that the load bearing elements are simple beams loaded in symmetrical three-point bending with a span of $2L$ and a cross section diameter D. The modulus of rupture M for this element is given in equation 3 where P is the maximum load carried by the individual fiber beam at rupture:

$$M = \frac{8PL}{\pi D^3} \tag{3}$$

Solving for P results in

$$P = \frac{\pi D^3}{8L} M \tag{4}$$

For a load applied in the x- or y-direction there are $1/2LD$ of these load carriers per unit area, giving a maximum stress of

$$\sigma_{max} = P\left(\frac{1}{2LD}\right) = \frac{\pi D^2 M}{16L} \tag{5}$$

in tension. Substituting equation 2 into equation 5 will give the dependence of tensile strength on the bulk density:

$$\sigma_{\substack{max \\ x,y}} = \frac{1}{\pi}\left(\frac{\rho_b}{\rho_t}\right)^2 M \tag{6}$$

For load applied in the z (stacking) direction the concentration of load bearing beams is $1/L$ per unit area and the maximum stress is given by

$$\sigma_{max} = \frac{8}{\pi 2}\left(\frac{\rho_b}{\rho_t}\right)^3 M \tag{7}$$

Equations 6 or 7 are solved for M, the modulus of rupture of a single fiber, by substituting known or measured values of σ_{max}, ρ_b, and ρ_t. The predicted moduli of rupture for the individual fibers tested are given in table XIV.

Table XIV.

Predicted Modulus of Rupture of Fibers
Using "Stack-of-Logs" Model

Tile	Stress Direction	σ , kN/m^2 (psi)	ρ_b , kg/m^3 (lb/ft^3)	M , MN/m^2 (psi)
Ames - AIM Silica	x - y plane	565 (82)	247 (15.4)	141 (20,495)
[one-directional forming]	z	220 (32)	247 (15.4)	193 (28,014)
[two-directional forming]	all directions	420 (61)	247 (15.4)	105 (15,246)
GE - REI Mullite	x - y plane	1310 (190)	200 (12.5)	483 (70,000)
MOD I	z	150 (22)	240 (15.0)	422 (61,160)

The modulus of rupture for glasses in general varies widely because of their extreme sensitivity to surface damage. Uniform abrasion of test specimens greatly reduces this variation and leads to lower values of the order of 69,000 kN/m^2 (10,000 psi). Heat treatment for short times at temperatures above 670 K (750°F) increases strength, a result which indicates that the presence of adsorbed water reduces strength (ref. 10). Since the processing of silica tile will obviously diminish the potential strength of the fiber, the predicted low values of M for silica are realistic.

In the case of mullite tiles, when crystallization is complete, the fibers consist of grains which usually are much less than 1 μm in diameter. For such a material, the modulus of rupture can be expected to be quite high if the density of the fiber approaches its theoretical value. Thus a value of 480 MN/m^2 (70,000 psi), as obtained, is not unreasonable.

EFFECTS OF DEVITRIFICATION ON TILE STRENGTH

Ainslie, et al. (ref. 11) report that fused silica rods about one millimeter in diameter were devitrified by growth of cristobalite crystals which had nucleated on the exterior surface and grew inward toward the center. They further note that, upon cooling,

> "... a rather coarse network of cracks begins to form due to the stresses that result from the difference between the thermal expansion coefficients of the fused silica and cristobalite. The specimen is still transparent, however, until cooled to about 250°C at which temperature the β-cristobalite transforms rapidly to the tetragonal α-cristobalite .... The α-cristobalite is usually full of cracks and defects and the grain size is considerably smaller than that of the β-cristobalite which formed originally...."

If small-diameter silica fibers follow the same behavior, it may be assumed that the effective diameter of the load-bearing cross section will be reduced in proportion to the volume fraction of cristobalite formed. Generally, the weight fraction is measured directly, but the volume fraction may be calculated by assuming the densities to be 2210 and 2300 kg/m^3 (2.21 and 2.33 g/cm^3) for the glass and the cristobalite, respectively. The new load-bearing diameter would be equal to the original diameter multiplied by $(1 - V_{fc})^{1/2}$, where V_{fc} is the volume fraction of cristobalite. When this new diameter is inserted in equation 4, keeping L and M for silica the same, the predicted P and also the predicted tensile stress are reduced by the factor $(1 - V_{fc})^{3/2}$. This model was applied to the data in figure 20 by multiplying the zero cristobalite strength by $(1 - V_{fc})^{3/2}$, and the results are shown by the solid line in figure 20. It is not known why the one average at 48% cristobalite is above that predicted by the model, while all others seem to agree. There is a significant probability, though, that the two high values are due to chance alone because they represent only 11% of the data points.

TILE SHRINKAGE

If it is assumed that fibers in the "Stack-of-Logs" model behave as though they were independent fibers, an expression for shrinkage rate can be derived:

$$\left(\frac{dS_L}{dt}\right)_T = \left(\frac{133.33}{n}\right)\left[\frac{\gamma}{D_o + \left(\frac{dD}{dt}\right)_T t}\right]$$

where: S_L = linear shrinkage (%)

D_o = initial fiber diameter

T = temperature.

Then, by letting T = 1530 K (2300°F), γ = 0.29 N/m (660 dynes/cm.), and $\eta = 6.32 \times 10^{10}$ Ns/m^2 (6.32×10^{10} Poises) and by using dD/dt = 0.0298 m/ks (0.107 μm/hr.), equation 8 results in

$$\frac{dS_L}{dt}\ (1530\ K) = \frac{0.612}{1.5 + 0.0298\,t} \qquad (9)$$

With this equation, the predicted shrinkage rates for 1530 K (2300°F) were determined; they are given in table XV. Table XVI shows the observed rates for various tiles at one hour.

From the rates calculated by means of equation 9, a numerical integration was performed in order to determine the values of shrinkage S_L. Figure 26 shows the results of this analysis with observed shrinkages from a specimen of LI-1542 (TT 139-6). The observed shrinkages were measured by two methods. The first was a method of continuous direct measurement of length while the specimens were being heated, and the second was a method of draw trials, i.e., measurements of dimensions before and after heat treatment. The fit of the observed data to the model appears to be very good.

Further confirmation of the validity of the model was obtained by determining the rates of linear shrinkages of several RSI silica tiles, as previously discussed, and determining the activation energies. Figure 18 presents Arrhenius plots for two LI-1500 tiles and one AIM tile. The

Table XV.
Isothermal Shrinkage Rates at 1530 K (2300°F)
as Predicted by Model

Time		dS_L/dt	
ks	(hr.)	s^{-1}	$(hr.)^{-1}$
0.0	(0)	0.408	(1.46)
1.8	(0.5)	0.394	(1.42)
3.6	(1)	0.381	(1.36)
7.2	(2)	0.357	(1.28)
14.4	(4)	0.317	(1.14)
28.8	(8)	0.260	(0.934)
57.6	(16)	0.190	(0.685)
115.2	(32)	0.124	(0.448)
∞	∞	0	0

Table XVI.

Shrinkage Rates Determined by Measurement
at about 1530 K (2300°F) for 3.6 ks (1 hour)

Tile Identification	Temperature K	dS_L/dt	Direction
AIM			
301-3	1526	0.44	x - y plane
301-2	1528	0.44	x - y plane
301-4	1530	0.60	x - y plane
LI-1542			
(TT-139-6)	1533	0.28	x - y plane
(TT 70-2)	1524	0.30	z direction
(TT 70-2)	1526	0.30	x - y

values obtained for E, the activation energy, compare very well with the values of 590 kJ/mole (141 Kcal/mole) observed for fused silica derived from a plot of viscosity versus temperature (ref. 5).

CONCLUSIONS

SUMMARY OF RESULTS

The materials improvement and optimization program resulted in measurable up-grading in properties of the fibers and of the tile studied. No specific or simple relationships were developed which related the devitrification of silica fibers to the type and amount of impurities and to temperature. It was determined that improvement of purity levels was necessary to reduce devitrification and that devitrification of silica fibers followed the normal free-energy relationships.

The degree of crystallinity developed due to flight-simulation temperatures was found to have significant effects upon two important properties of the tile, shrinkage and strength. Devitrification of silica fibers materially decreased the shrinkage of the tile, but it must be kept at a minimum (less than 5 to 7 percent) after thermal cycling in order to maintain adequate mechanical properties. This sensitivity of mullite tile to fiber crystallinity was not observed as higher strengths were attained when the crystallization of mullite was complete and less shrinkage occurred. Furthermore, thermal cycling of mullite tiles had little or no effect upon either property. Thermal cycling which simulated re-entry conditions resulted in an increase in the crystallinity and the porosity of tile coatings.

A model was developed whereby the tensile strength of silica tile can be predicted from data on the weight fraction of cristobalite present and

the density of the tile. The shrinkage rate of the tile can be predicted using a second model based upon the fiber diameters and exposure temperature.

CONCLUDING REMARKS

Attempts were made in this study to make a simple linear relationship between the amount and type of impurity and the temperature. These were not successful. The impact of devitrification upon the properties of silica RSI is of such importance as to warrant further study of these inter-relationships. Impurities related both to processing and to environment should be considered.

Ceramic Engineering Division
University of Washington
Seattle, Washington 98195
July 21, 1975

REFERENCES

1. Second Quarterly Progress Report, Contract NAS 2-6541, Appendix I, Ceramic Engineering Division, University of Washington, July 30, 1972.
2. Second Quarterly Progress Report, Contract NAS 2-6541, Appendix II, Ceramic Engineering Division, University of Washington, July 30, 1972.
3. Seventh Quarterly Progress Report, Contract NAS 2-6541, Appendix B, Ceramic Engineering Division, University of Washington, May 2, 1973.
4. Third Quarterly Progress Report, Contract NAS 2-6541, 3-11, Ceramic Engineering Division, University of Washington, March 31, 1972.
5. Elmer and Nordberg, Corning Research, 1961, 225-238, (1961). (Reprinted from Sixth Symposium on the Art of Glassblowing, 1961.)
6. Heatherington, et al., Phys. Chem. Glass, 5(5), 130-36, (1964).
7. Seventh Quarterly Progress Report, Contract NAS 2-6541, 12-18, Ceramic Engineering Division, University of Washington, May 2, 1973.
8. Van Vlack, Physical Ceramics for Engineers, p. 152, Addison-Wesley, 1964.
9. Ormiston and Whittemore, "Sintering of Silica Fiber Compacts," Amer. Ceram. Soc. Bul., 52 (3), 247-249, (1973).
10. Condon, "Physics of the Glassy State III. Strength of Glass," Am. J. Phys., 22(4), 224-232, (1954).
11. Ainslie, et al., "Devitrification Kinetics of Fused Silica," Nucleation and Crystallization Symposium, Reser, Smith, and Insley, eds., American Ceramic Society, Columbus, Ohio, pp. 97-107, (1962).

Three theses, submitted in partial fulfillment of the requirements for the degree of Master of Science in Ceramic Engineering at the University of Washington in 1972, resulted from support made available by this contract.

T. J. Ormiston, The Sintering of Silica Fiber Compacts.

P. K. Khandelwal, Mechanical Properties of Hard Compacted Refactory Fiber Insulation.

S. H. Garofalini, Crystallization Kinetics of a Sodium - Doped Colloidal Silica.

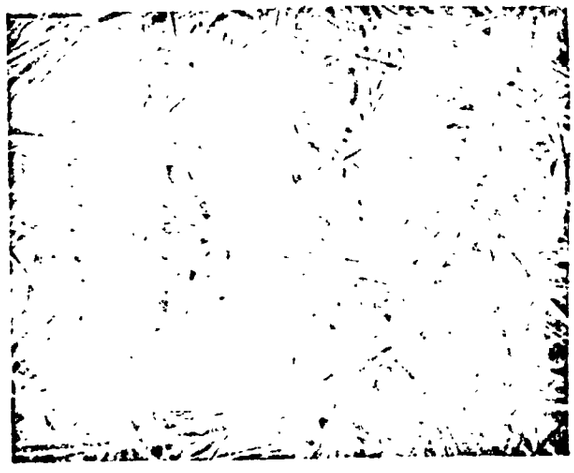

a. 475X

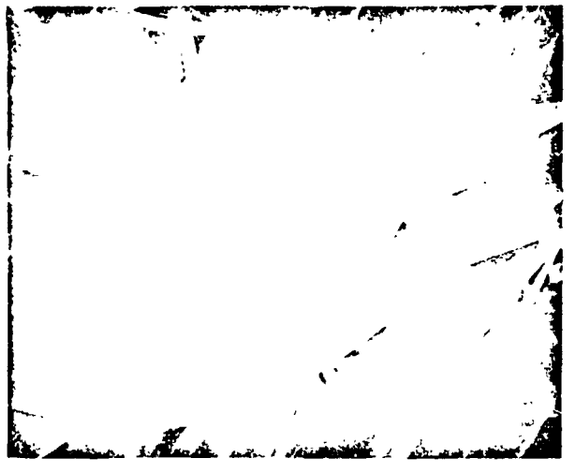

b. 2550X

Figure 1. - SEM photomicrographs of "as-received" Microquartz fibers.

a. 190X

b. 2025X

Figure 2. - SEM photomicrographs of "as-received" mullite fibers.

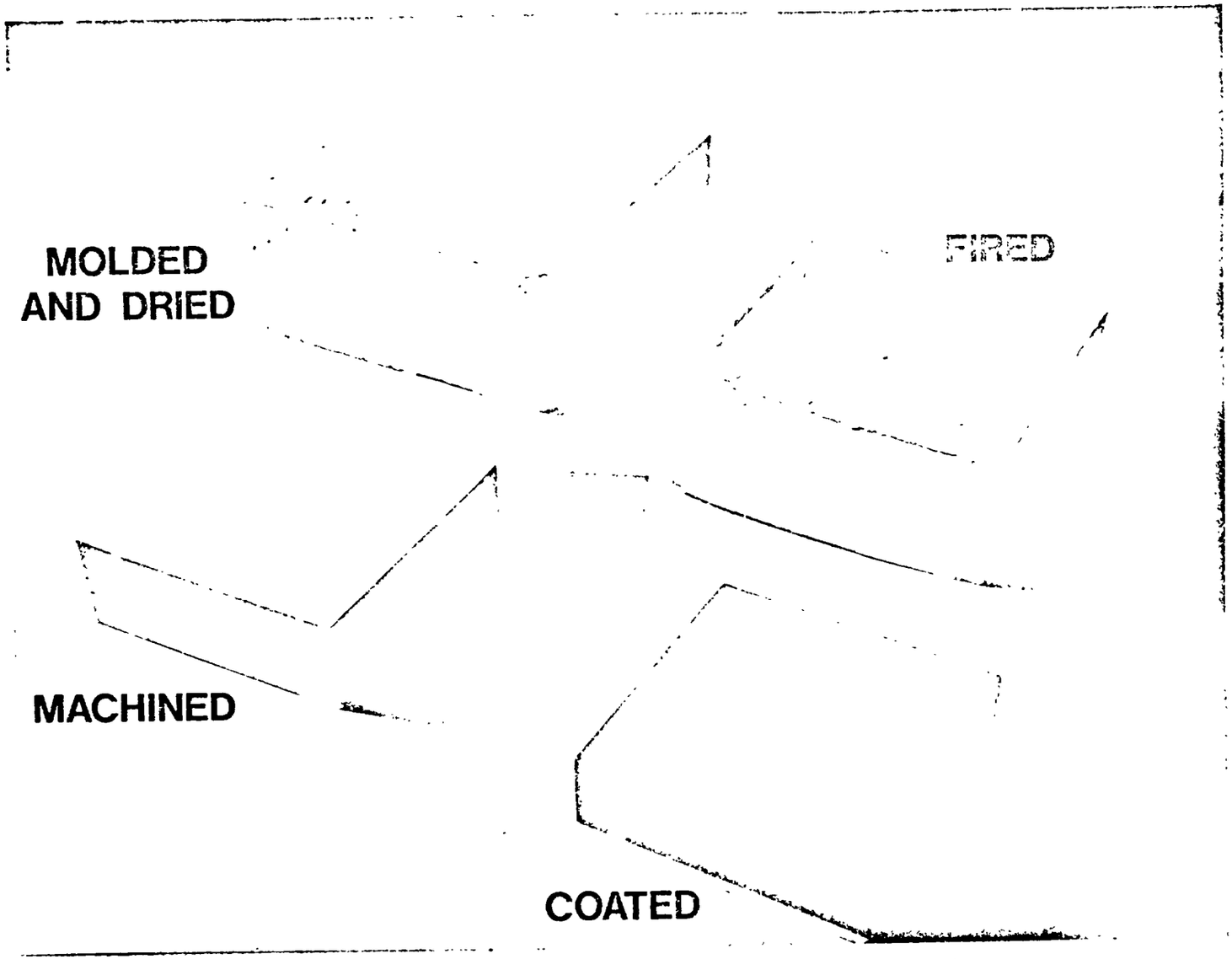

Figure 3. - AIM tile in the principal steps in processing.

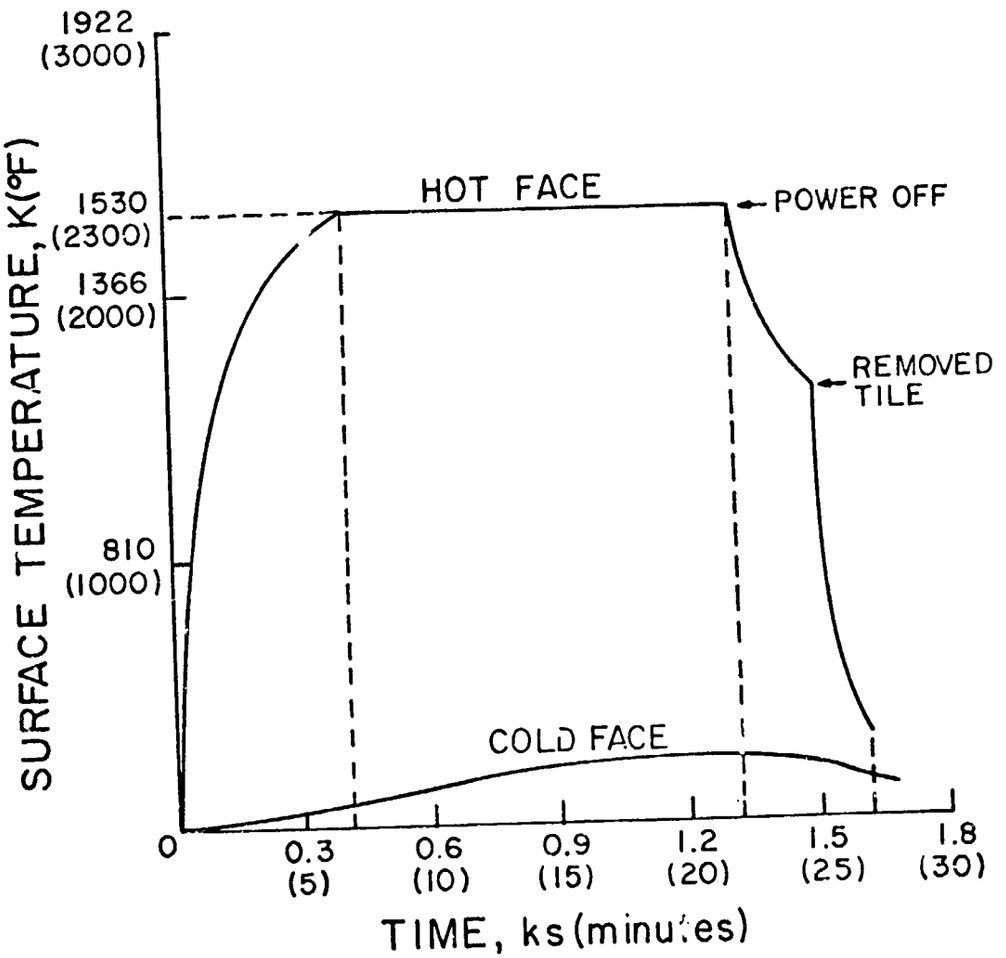

Figure 4. - Time - temperature curve for simulated re-entry heating.

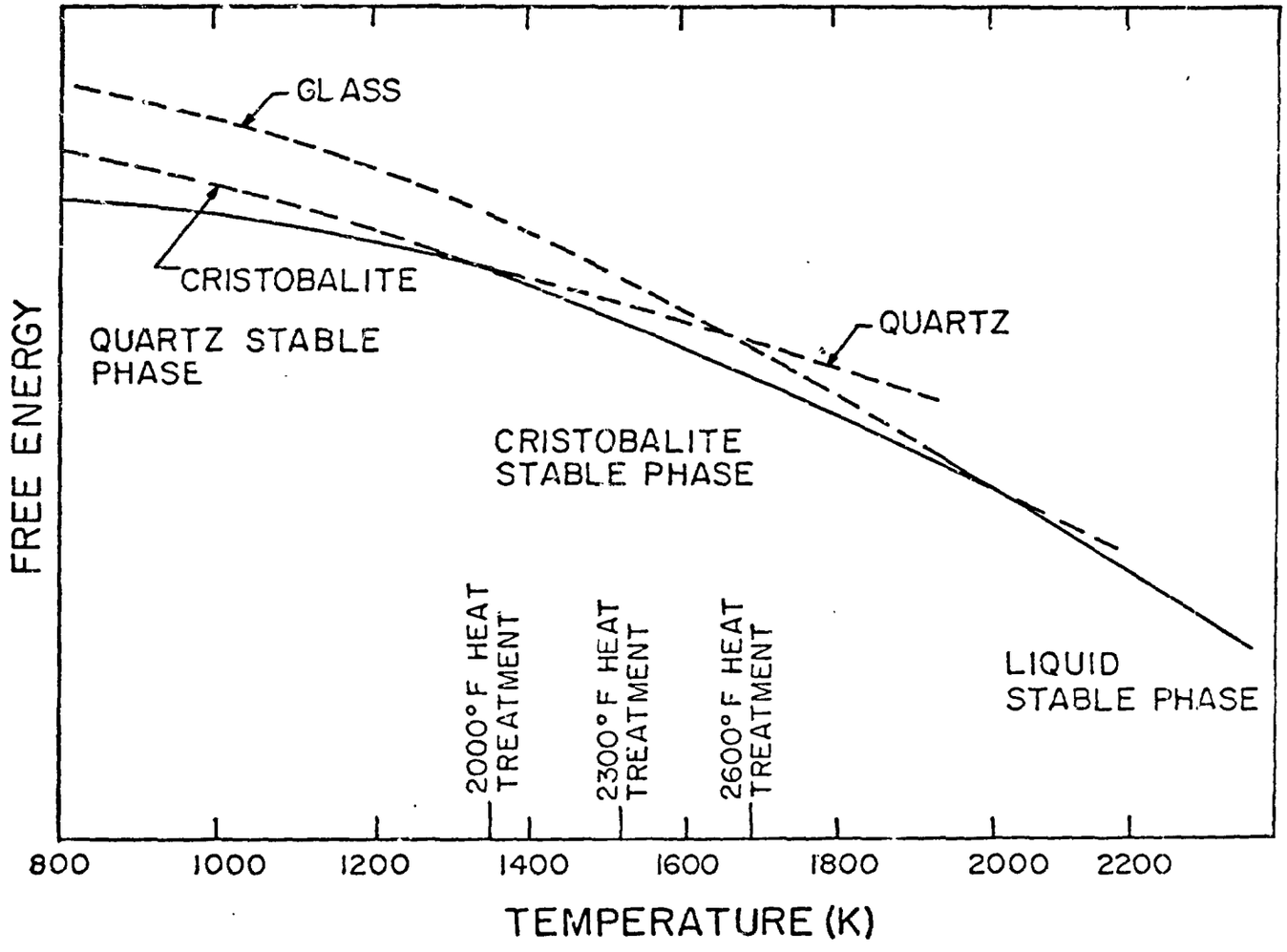

Figure 5. - Relative free energy of various forms of silica.

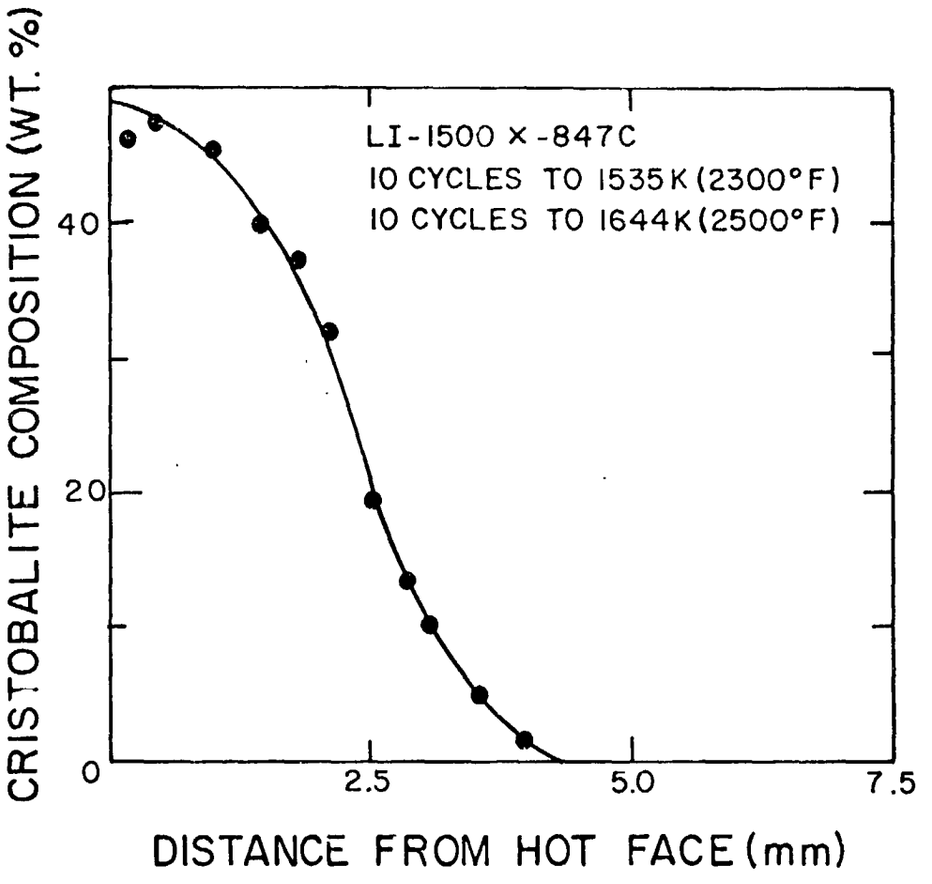

Figure 6. - Effect of twenty thermal cycles on depth of devitrification of LI-1500.

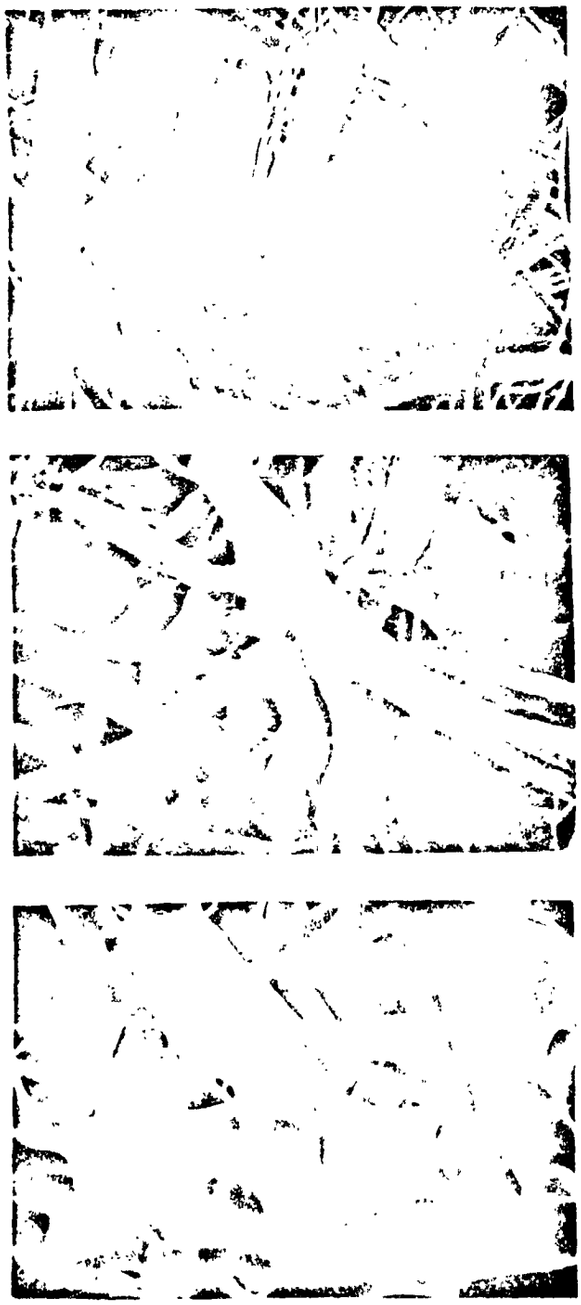

a. "As-received"

1800X

b. 57.6 ks at 1255 K
(16 hrs. at 1800°F)

2000X

c. 57.6 ks at 1700 K
(16 hrs. at 2600°F)

2000X

Figure 7. - SEM photos showing effects of isothermal heating on Microquartz, Lot 1466.

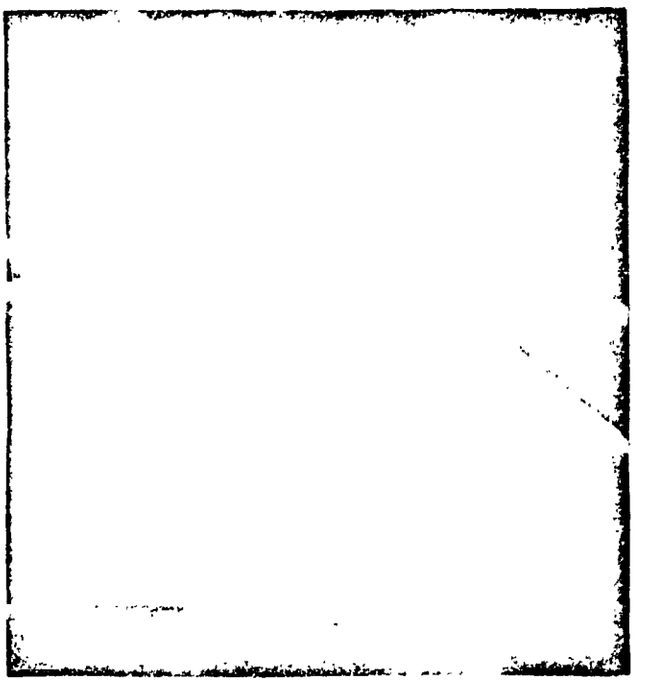

a. "as-received"

11,000X

Figure 8. - SEM photos showing effects of isothermal heating upon morphology of Microquartz fiber, Lot 1437.

b. 57.6 ks at 1700 K
(16 hrs. at 2600°F)

2040X

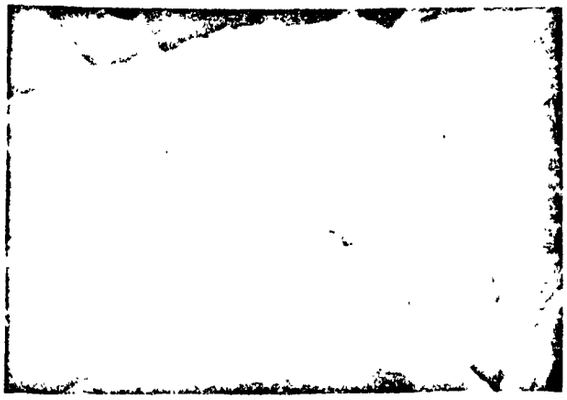

c. 57.6 ks at 1700 K
(16 hrs. at 2600°F)
HF etch

6400X

d. 57.6 ks at 1700 K
(16 hrs. at 2600°F)
HF etch

Figure 8. (Continued).

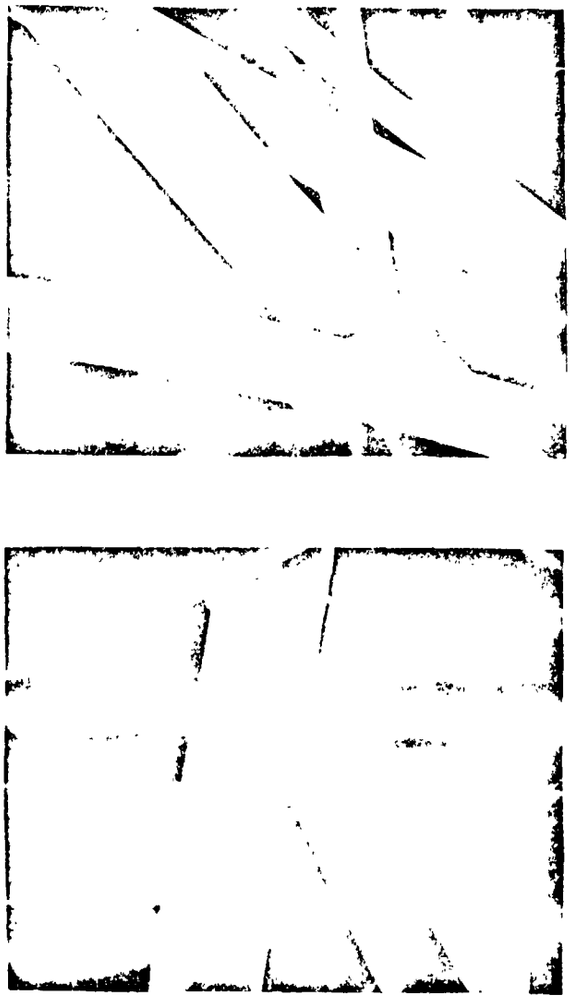

a. "as-received"

2075X

b. 57.6 ks at 1700 K
(16 hrs. at 2600°F)

2450X

Figure 9. - SEM photos showing effects of isothermal heating upon morphology of mullite fibers, Lot S-98-E.

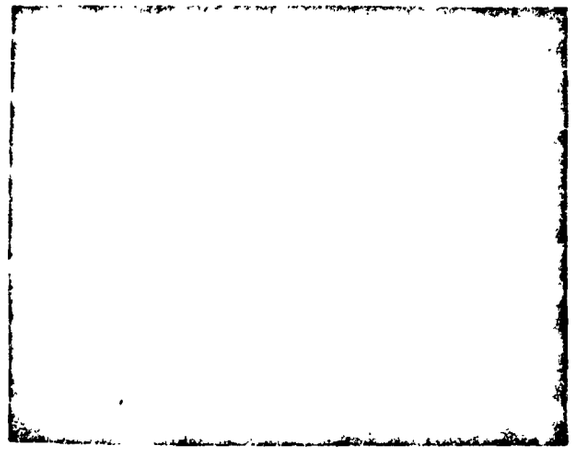

a. Surface of fiber

50,000X

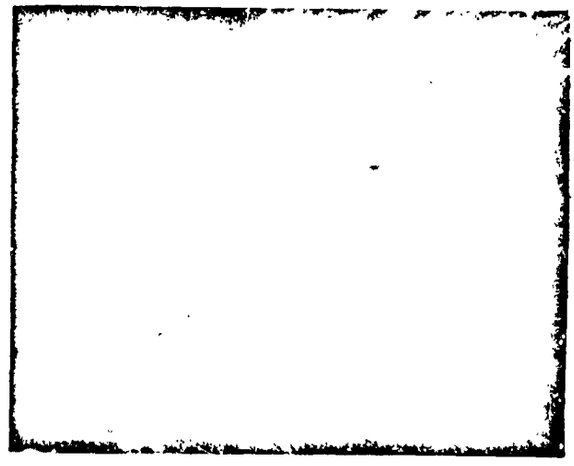

b. Fracture surface of fiber

20,000X

Figure 10. - SEM photos showing crystallization of mullite after isothermal heating for 57.6 ks at 1700 K (16 hrs. at 2600°F).

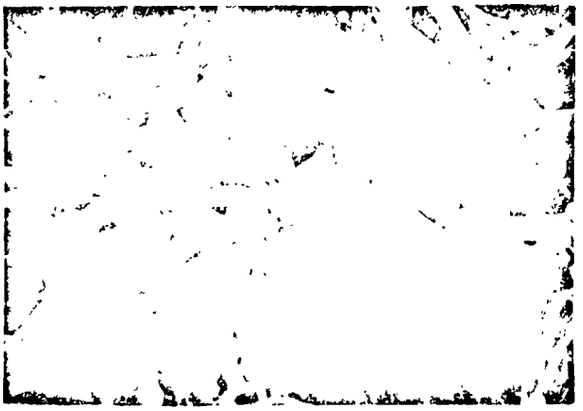

a. 1000X

b. 5000X

c. 20,000X

Figure 11. - SEM photos showing bonding in LI-1500.

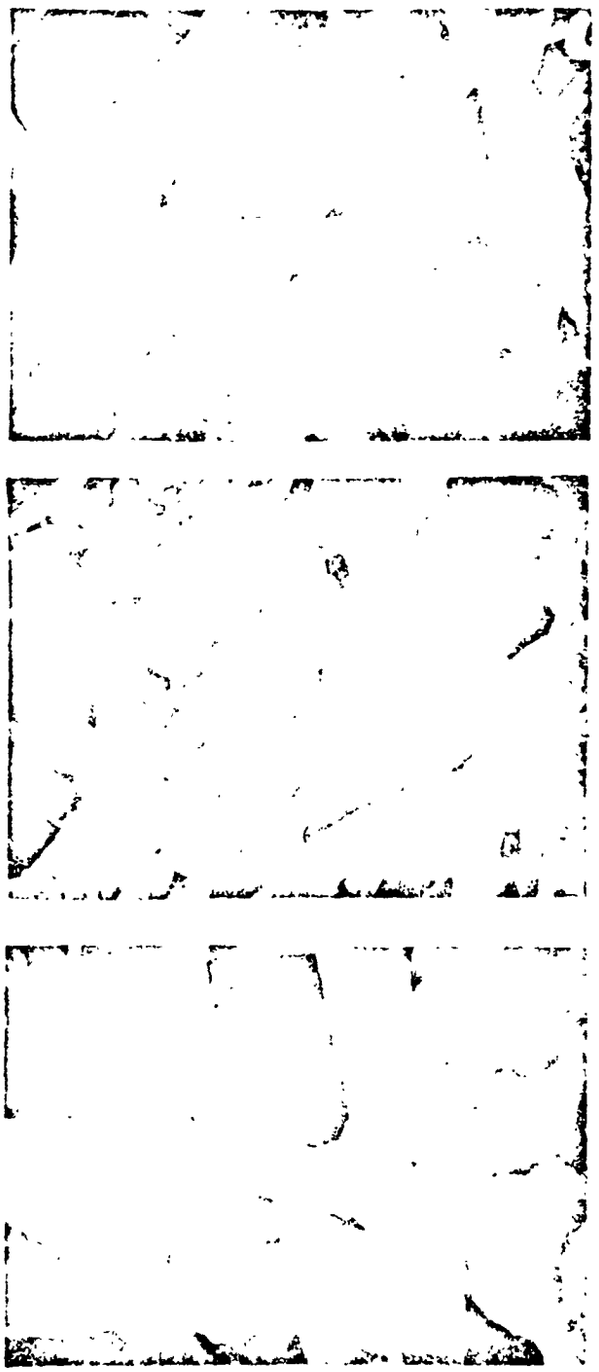

a. 2000X

b. 2200X

c. 5000X

Figure 12. SEM photos showing bonding in LI-1500.

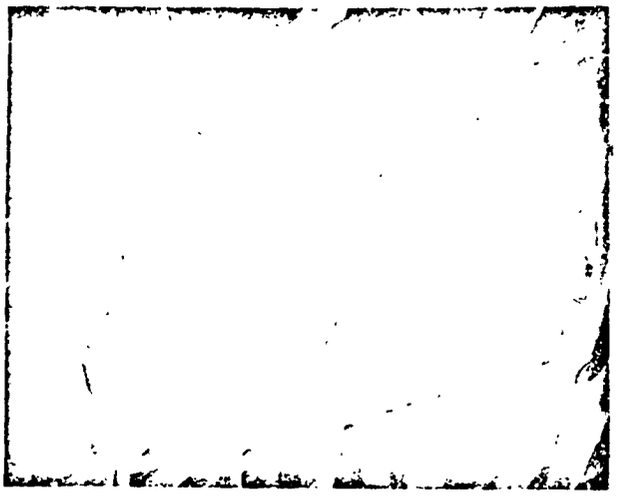

a. 2125X

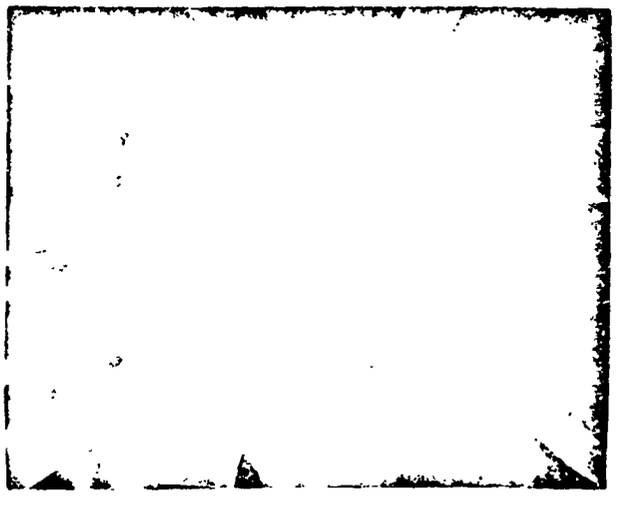

b. 5380X

Figure 13. - SEM photos showing bonding in AIM billet #46.

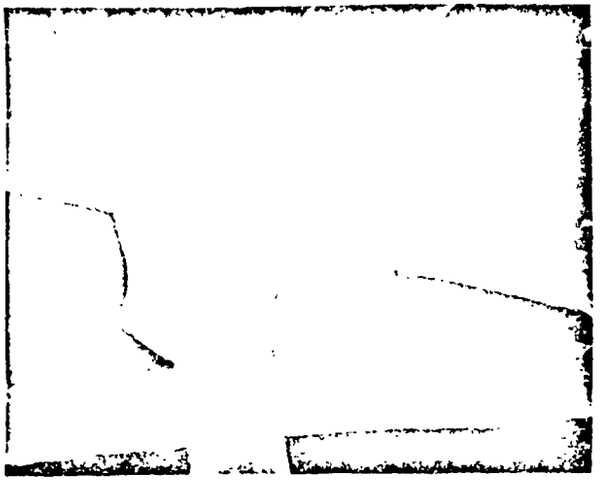

a. 2,000X

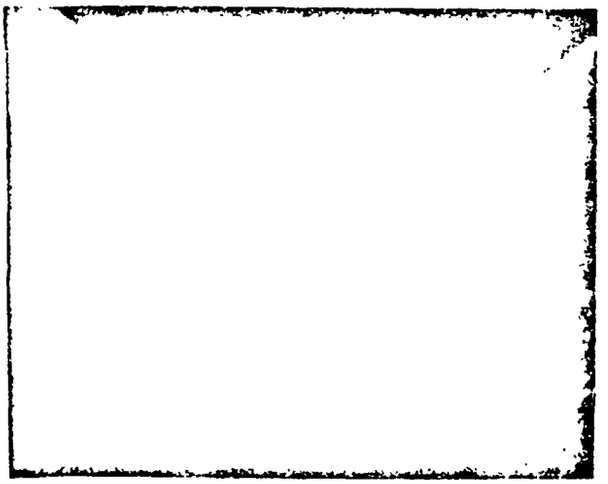

b. 20,000X

Figure 14. - SEM photos of HCF showing glass fillet bonding.

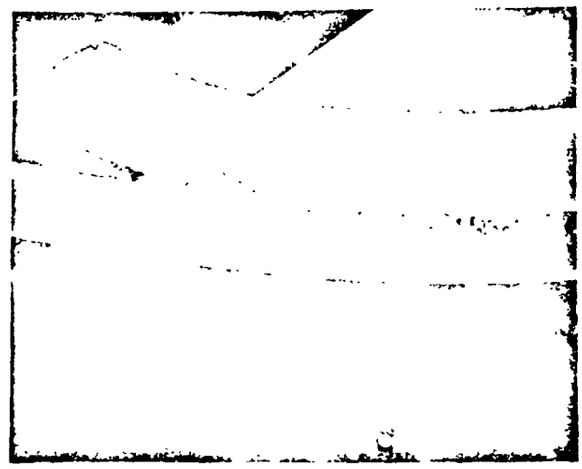

a. 2000X

b. 10,000X

Figure 15. - SEM photos of HCF showing crystalline fillet bonding.

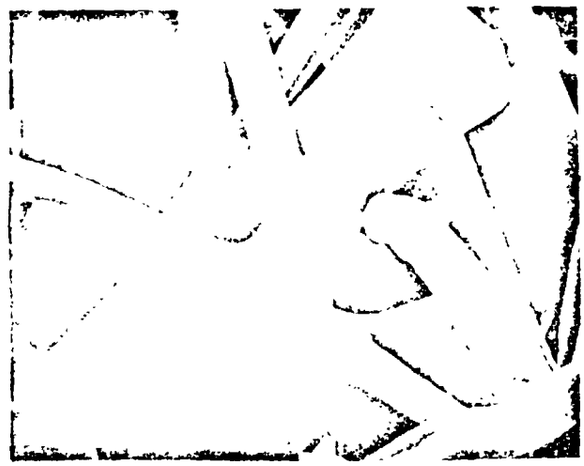

a. 1100X

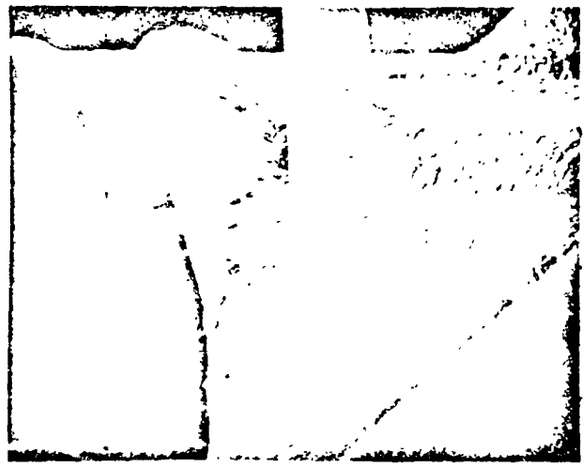

b. 2200X

Figure 16. - SEM photos of REI JG-53 showing glass-crystalline fillet bonding.

a. 100X

b. 250X

Figure 17. - SEM photos of HCF showing Eccospheres and their bonding effect on mullite fibers.

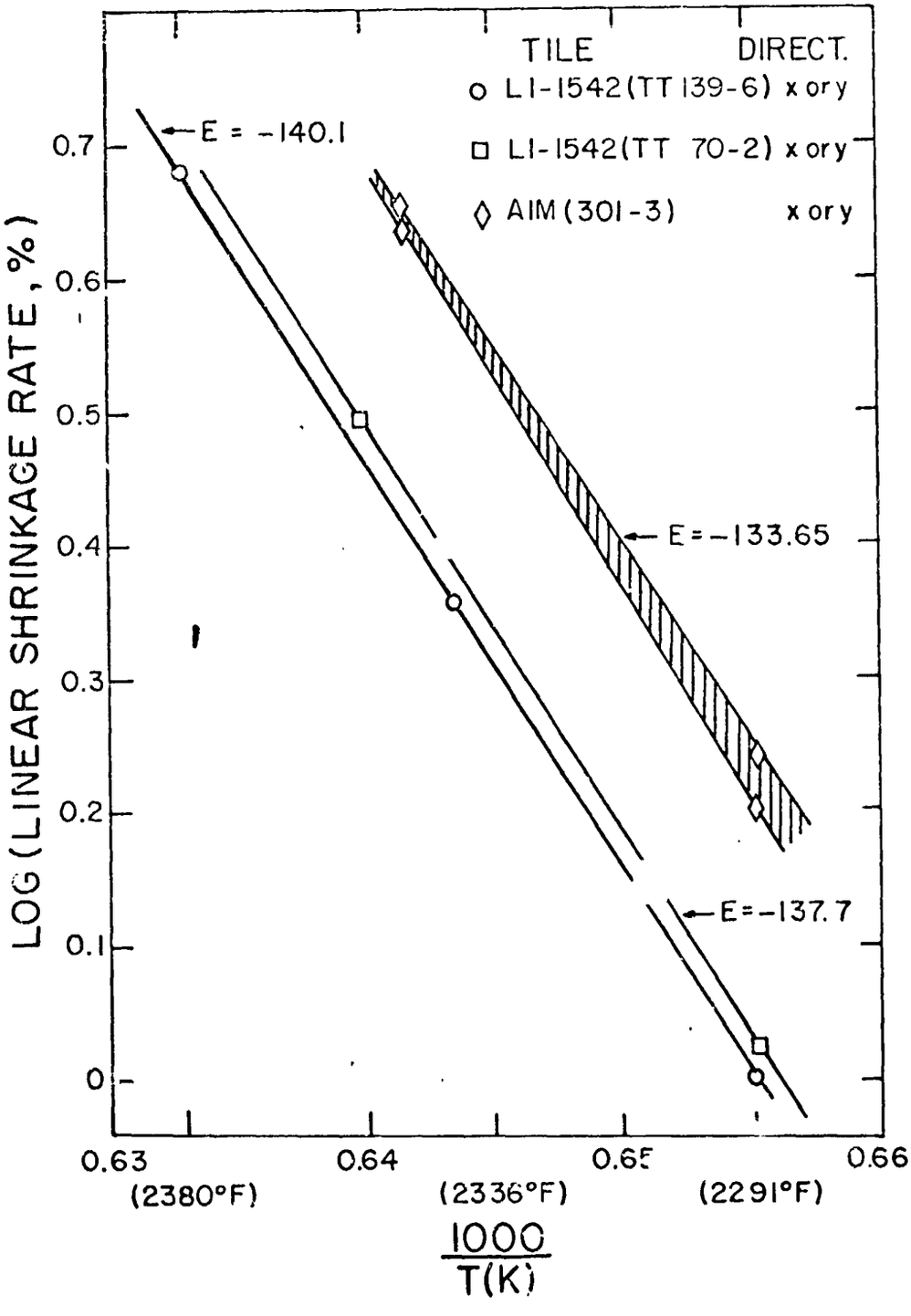

Figure 18. - Arrhenius plots of shrinkage vs. time for silica RSI.

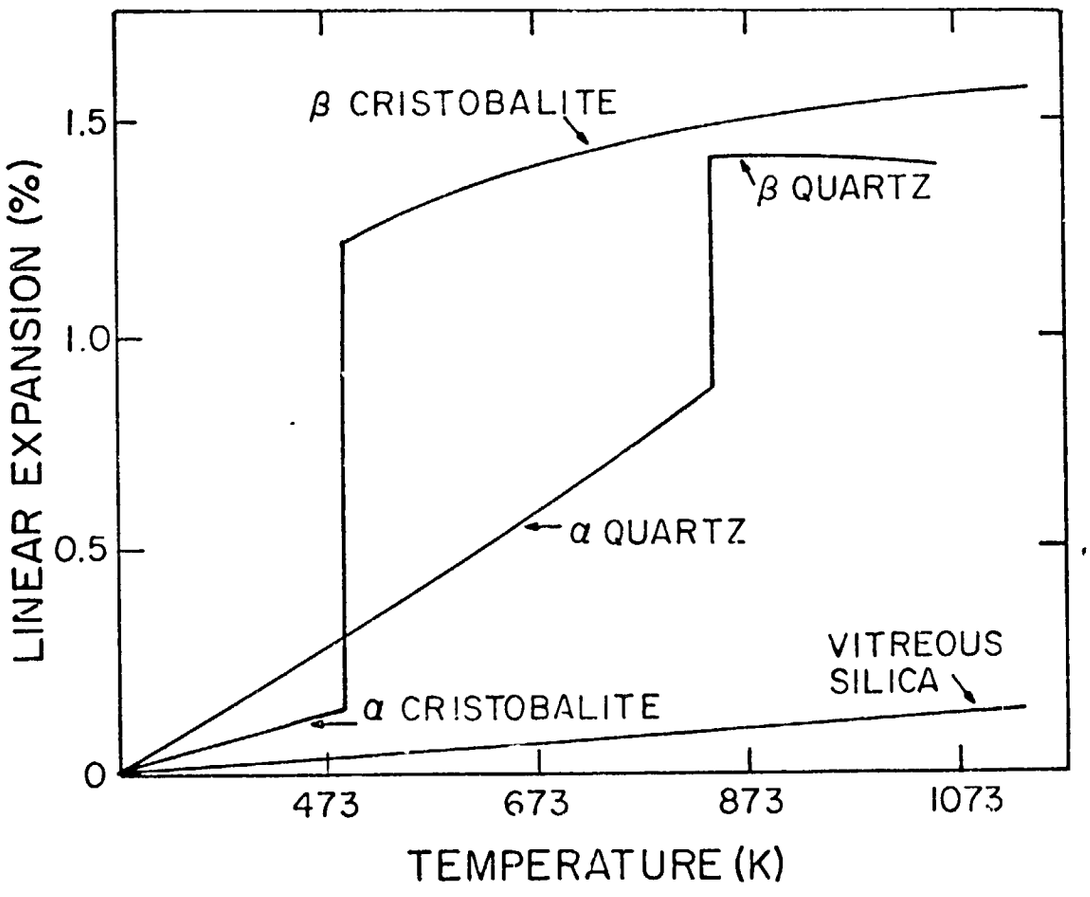

Figure 19. - Linear thermal expansion of several forms of silica (ref. 8).

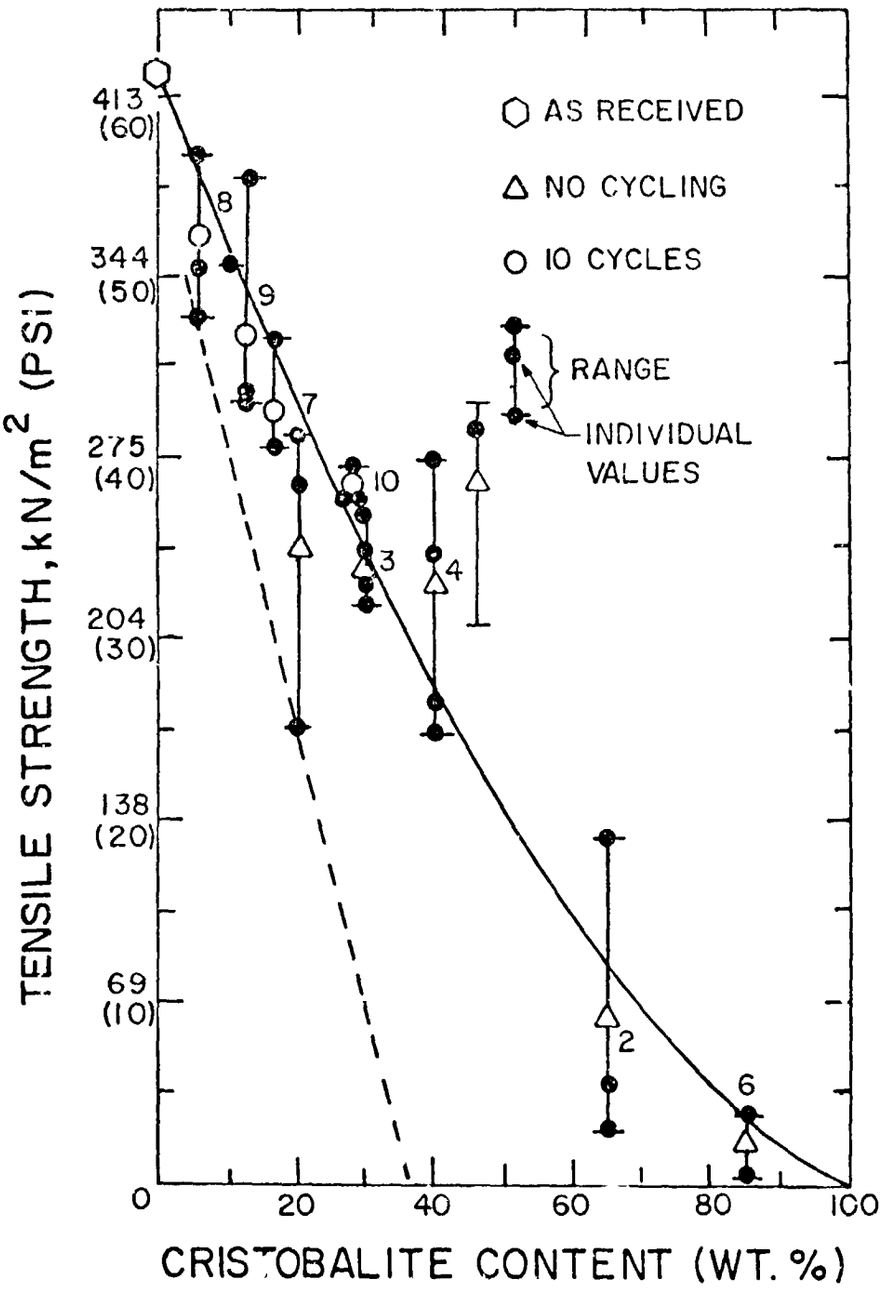

Figure 20. - Effects of cristobalite content and low temperature cycling on the tensile strength of AIM tiles.

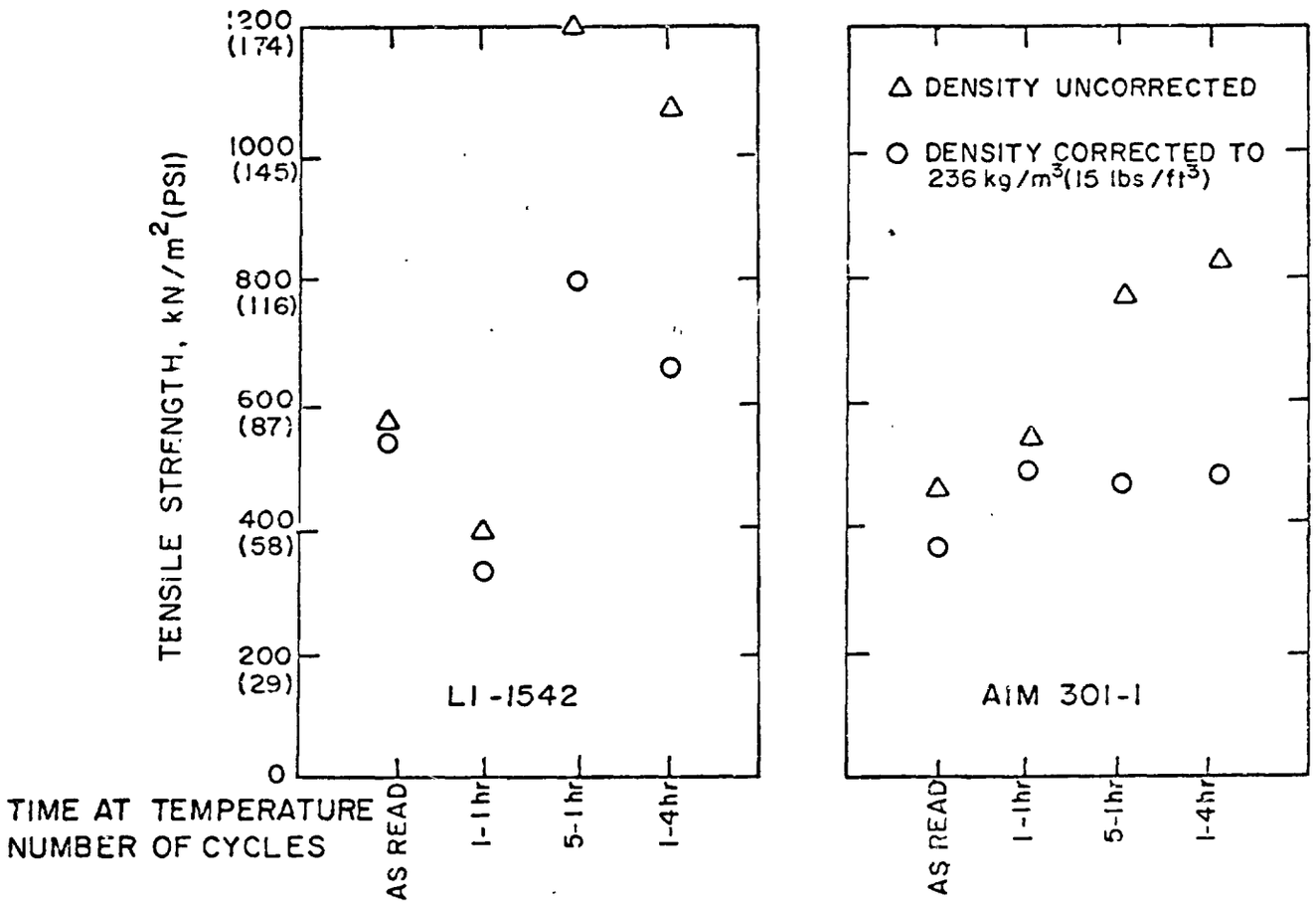

Figure 21. - Effect of isothermal cycling on tensile strength of silica RSI.

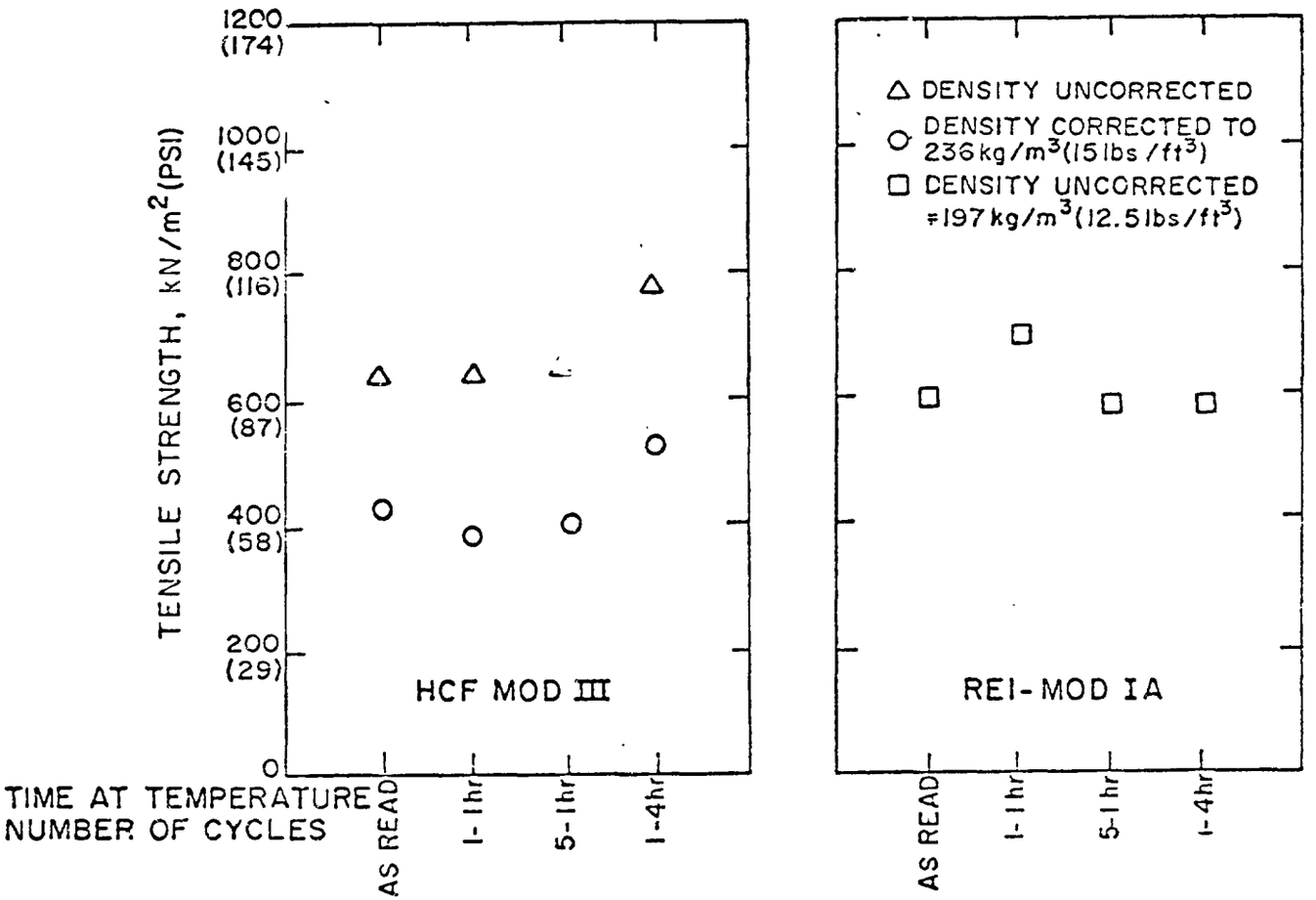

Figure 22. - Effect of isothermal cycling on tensile strength of mullite RSI.

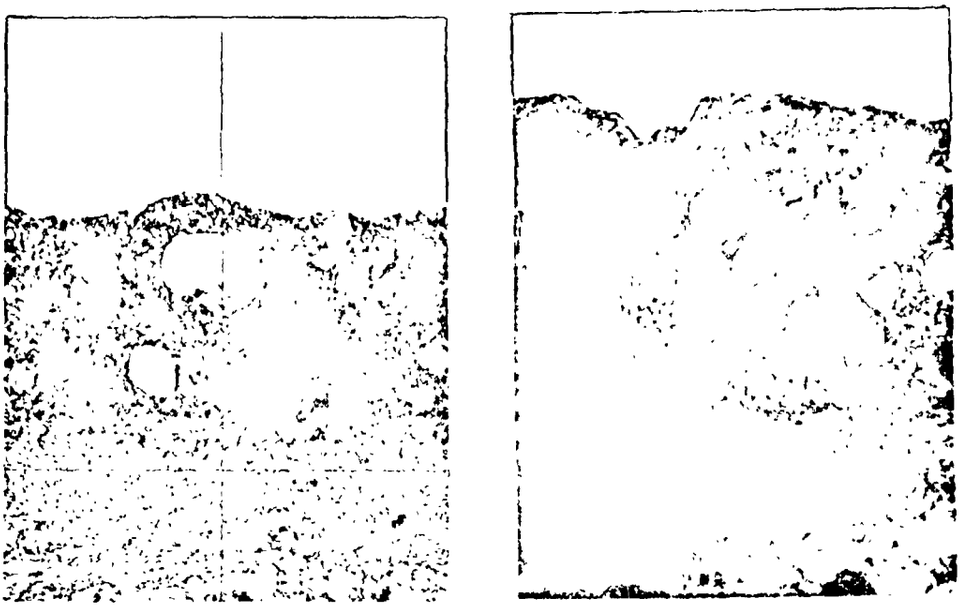

a. "as-received

135Z

b. After 10 isothermal cycles to 1520 (2300°F,

Figure 23. - Light optics thin section photomicrography.

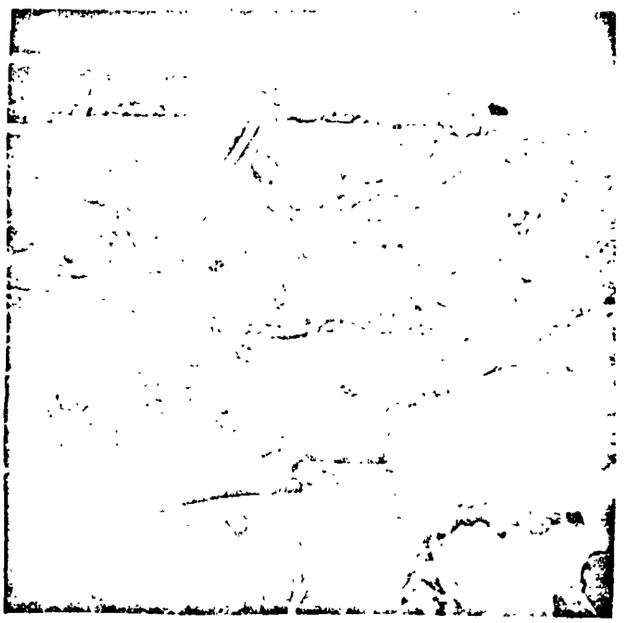

Figure 24. - SEM photo of "as-received" MDAD Mod I coating and interface.
216X

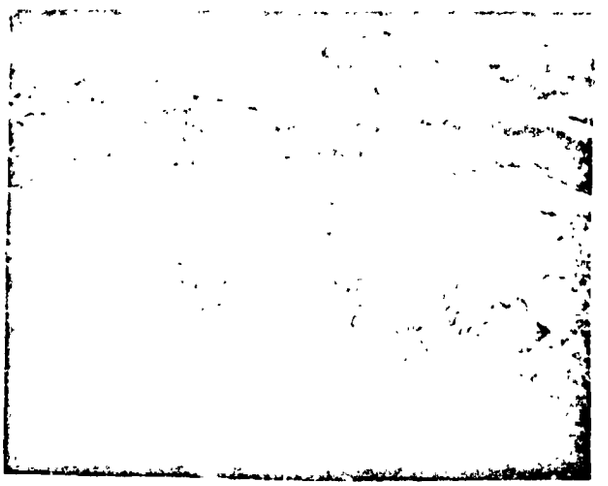

a. "as-received"

50X

b. After 10 cycles of isothermal heating to 1520 K (2300°F)

Figure 25. - SEM photo showing cross section of MDAC Mod III coating (top layer spalled off during sample preparation).

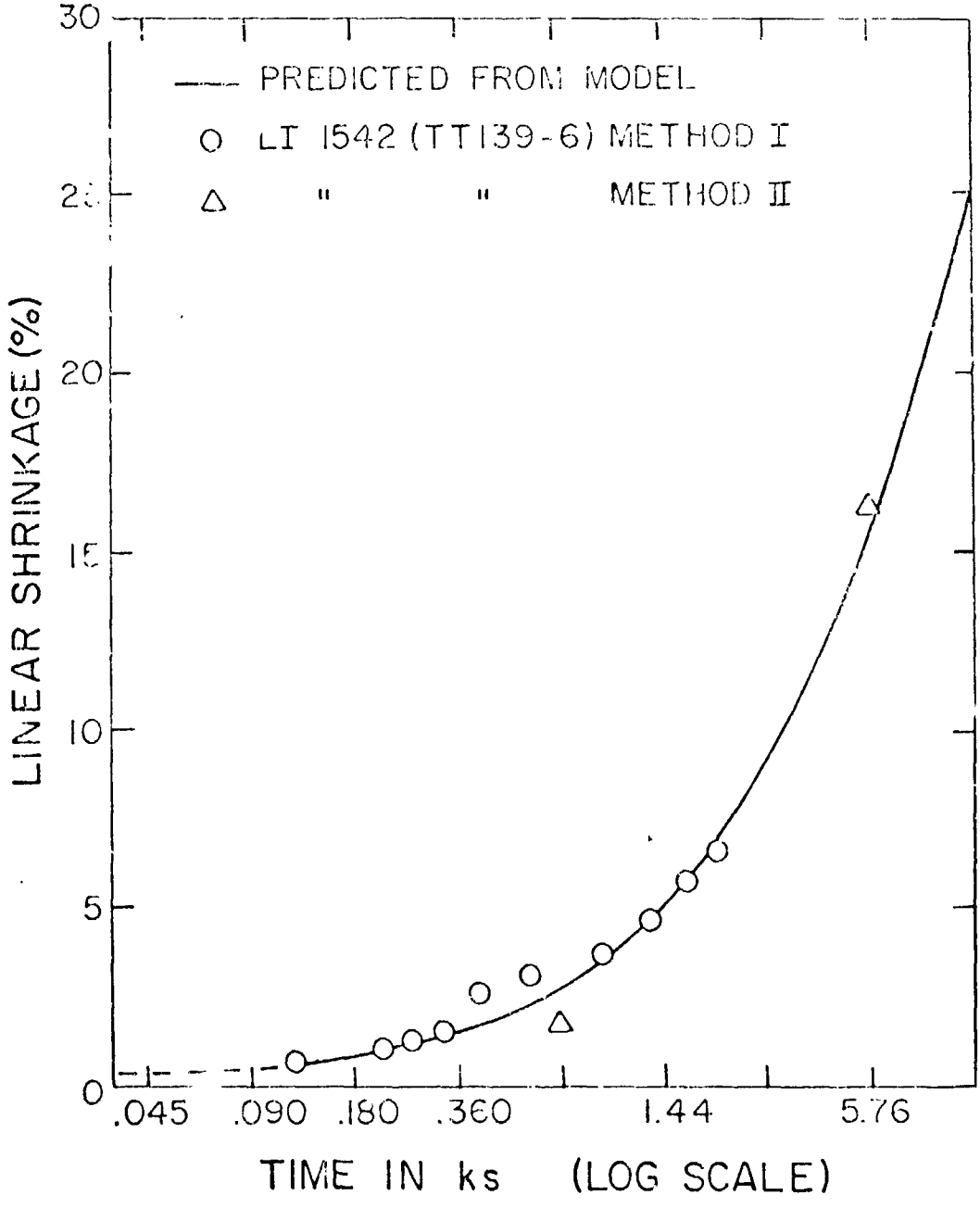

Figure 26. - Comparison of observed shrinkage in LI-1542 with shrinkage values predicted by model.